Bulletin of Earthquake Engineering (2022) 20:3077–3116
https://doi.org/10.1007/s10518-021-01241-7

S.I. : SOIL-STRUCTURE INTERACTION EFFECTS ON THE DYNAMICS OF STRUCTURES

Assessment of SSI effects on stiffness of single and grouped helical piles in dry sand from large shake table tests

A. F. Fayez[1] · M. H. El Naggar[1] · A. B. Cerato[2] · A. Elgamal[3]

Received: 20 January 2021 / Accepted: 24 September 2021 / Published online: 13 October 2021

Abstract
Full-scale shake table testing was conducted to evaluate the seismic performance of single and grouped helical piles. Eight circular and one square helical piles with different properties including length, radius and number of helices, as well as one driven circular pile were installed in dry sand enclosed in a laminar soil shear box that was situated on the shaking table. Dynamic properties of sand bed and its natural frequencies as well as natural frequencies of single and grouped helical pile-soil systems were evaluated from the collected data during different shaking events. The effects of different pile configurations as well as successive shakings on the natural frequencies of the sand bed and pile-soil systems were also investigated. It was found that the soil's disturbance increased as number of helices increased, which resulted in reduced pile-soil stiffness and natural frequency. Natural frequencies of single piles and pile groups decreased due to successive shakings owing to the degradation in the pile-soil stiffness and gap forming around pile shafts near the ground surface. The pile's free length significantly reduced the stiffness of single and grouped helical piles and gap opening further increased the free length and hence resulted in additional reduction in stiffness and natural frequencies. These effects must be considered in seismic design of helical pile foundations. Furthermore, the seismic responses of single and grouped helical piles are greatly affected by the resonance condition, which causes large soil deformations and significant reduction in the stiffness of the pile-soil system. It was also demonstrated that the software DYNA6 could predict the single and grouped piles behaviour correctly by accounting for degradation of the soil's stiffness and gap opening.

Keywords Helical piles · Seismic response · Shake table · Soil-pile interaction · Group behaviour

✉ M. H. El Naggar
naggar@uwo.ca

Extended author information available on the last page of the article

1 Introduction

In recent years, helical piles have become an attractive alternative to conventional foundations due to their ease and rapid installation, efficient use of material and the ability to estimate their axial capacity from installation torque measurements (Perko 2009). Owing to their configuration, which comprises a straight steel shaft with one or more helices, helical piles can be designed to place the load bearing helical plates below soft or liquefiable soil to ensure acceptable performance and capacity during and after an earthquake. Recent advances in helical pile installation equipment promoted the use of large diameter helical piles installed to large depths to achieve large capacity for supporting high-rise buildings, bridges and offshore installations.

Helical piles offer safe and cost-effective foundation solutions for supporting structures in earthquake prone regions. They have performed well during recent large earthquakes (Cerato et al. 2017). Anecdotal evidence from recent earthquakes in Christchurch, New Zealand (2011, 2012) and Alaska, USA (2016, 2018) revealed that structures supported on helical piles withstood earthquakes with limited or no structural damage. For example, Anchorage, Alaska, experienced back-to-back earthquakes and aftershocks of 7.0 and 5.7 magnitudes that damaged public buildings and houses causing significant foundation settlement, which damaged many structures. However, structures supported by helical piles remained intact and level. Surveys conducted after the earthquake revealed that all structures supported by helical piles have not experienced any damage or settlement due to the earthquake (Techno Metal Post n.d.).

In seismic regions, helical piles are designed to sustain both axial and lateral loading. Helical piles' performance and design for axial loading are well investigated (Livneh and El Naggar 2008; Sakr 2009, 2011; Tsuha et al. 2012; Bagheri and El Naggar 2013, 2015; Elkasabgy and El Naggar 2013, 2015; Elsherbiny and El Naggar 2013; Gavin et al. 2014; Ridgley 2015; Fahmy and El Naggar 2016a, 2017; Harnish and El Naggar 2017; Schiavon et al. 2017, 2019; El Sharnouby and El Naggar 2018a; Guo and Deng 2018; Li et al. 2018; Perez et al. 2018; Lanyi-Bennett and Deng 2019; Li and Deng 2019; Nabizadeh and Choobbasti 2019; Alwalan and El Naggar 2020a,b). Many of these studies demonstrated that the axial capacity of helical piles is equal to or greater than that of an equivalent driven steel pile owing to the additional load carrying capacity offered by the helices.

The performance of single helical piles under lateral static, cyclic or seismic loading has attracted significant attention recently owing to the interest in their use in wind turbine foundations, offshore projects and to support structures subjected to earthquake loading. For example, Fahmy and El Naggar (2016b), Elsherbiny et al. (2017), El Sharnouby and El Naggar (2018a), Elkasabgy and El Naggar (2018, 2019) conducted full-scale helical pile loading programs involving static, cyclic or dynamic load tests. These studies demonstrated that the performance of helical piles under lateral loading is primarily governed by the soil's resistance along the upper portion of the pile shaft, same as the case for driven piles.

Most of the full-scale cyclic and dynamic loads were applied at the pile's head using mechanical actuators/shakers, which only represents the inertial loading conditions. Thus, these studies did not account for the kinematic soil-pile interaction. These alternative loading schemes are pursued because large shake table testing opportunities are rare and expensive. At the same time, Fleming et al. (2015) and Elkasabgy and El Naggar (2018) argue that scaled models and field-scale cyclic and dynamic loading applied to the pile's head still allow reasonable simulation of its dynamic behaviour.

The seismic response of pile groups is governed by their dynamic characteristics, which are influenced by soil-structure interaction (Stewart et al. 2012). The pile-soil interaction and group effects are governed by the properties of the soil and the piles as well as the group configuration (Miura 1997; Boulanger et al. 1999; Jeremic et al. 2009). In addition, the characteristics of the supported structure may influence the soil-structure interaction effects (Badry and Satyam 2017). These effects are generally significant for rigid structures supported by relatively flexible foundations (Mylonakis and Gazetas 2000; Givens et al. 2012; Carbonari et al. 2017; Michel et al. 2018).

The pile-soil interaction under earthquake loading have been examined through scaled models (i.e., 1 g and centrifuge models) in controlled laboratory setting (Moss et al. 1998; Bhattacharya et al. 2011; Motamed et al. 2013; Albaghdadi et al. 2015; Newgard et al. 2019). However, Kagawa et al. (2004) listed several limitations of centrifuge simulation of seismic response of soil-pile-structure systems, including scaling issues, variation of centrifuge acceleration within the model and boundary effects. On the other hand, full-scale shaking table facilities with large capacity actuators allow testing of almost full-scale piles and pile groups. There are a few well-documented seismic studies of pile groups employing full-scale shake table tests. Shirato et al. (2008) examined the seismic response of 3×3 pile group embedded in dry sand employing large-scale shake table testing. Furthermore, Xu et al. (2020a, b) evaluated the response and failure mechanism of a large-model pile group involving 2×2 piles installed in liquefiable and non-liquefiable sand. However, none of these studies examined the seismic performance of helical piles. In addition, the group behaviour of helical piles under seismic loading has never been examined.

This literature review collectively indicates the clear advantages of helical piles and their significant potential as a viable and efficient foundation option in seismic regions. It also shows that full-scale testing provides the most realistic representation of the piles and shake table testing is an excellent means to investigate their seismic performance. However, there is a lack of realistic full-scale testing studies for grouped helical piles involving actual seismic loading. Therefore, in order to better understand the seismic response of grouped helical piles and to provide the basis of robust analytical and numerical models, the authors have undertaken a comprehensive large-scale shake table testing study of single and grouped helical piles. The test program was performed employing the Large High Performance Outdoor Shake Table (LHPOST) located at The University of California – San Diego. Some aspects of this testing program have been already published in several articles. Elsawy et al. (2019a, b) evaluated the seismic performance of single helical piles in comparison with steel driven piles and presented detailed descriptions of the data reduction methods for interpreting the measured responses during the tests. In addition, Shahbazi et al. (2019) investigated the damping characteristics of grouped helical piles in dense sands under small and large shaking events. Furthermore, Shahbazi et al. (2020) analyzed the experimental observations to evaluate the structural natural frequency and pile-group stiffness, and used the experimental results to calibrate a numerical model that was then used to conduct a parametric study to gain a broader understanding of the seismic behavior of structures supported by helical pile groups under varying conditions. This study evaluates the effects of SSI on the dynamic stiffness and natural frequencies of single and grouped helical pile-soil systems from the collected data during different shaking events. The effect of different pile and/or soil configurations is investigated. Moreover, the effect of successive shakings on the stiffness and natural frequencies of the piles and the soil mass is also explored through the variation of these properties during the testing program. Finally,

an analytical approach is proposed to simulate the dynamic characteristics of helical piles accounting for degradation of the soil's stiffness and gapping at the pile-soil interface.

2 Experimental setup

The testing program conducted to realistically represent the seismic loading of helical piles and provide essential information regarding the dynamic behaviour of single and grouped helical piles is summarized herein. Single and grouped helical piles were installed in a dry dense sand bed enclosed in a laminar box situated on the 12 m by 7.6 m Large High Performance Outdoor Shake Table (LHPOST) at the University of California – San Diego (UCSD). Five testing stages were carried out during this research program: Testing Day 1 (TD1) involved sand bed shaking; Testing Day 2 (TD2) included testing of single piles with no inertial masses; Testing Day 3 (TD3) included single piles shaking with inertial masses mounted on their heads; Testing Day 4 (TD4) involved pile group shaking with presumed fixed head connections supporting a model structure; and Testing Day 5 (TD5) encompassed pile group shaking with pinned head connections supporting the model structure.

The dry sand bed was placed into the laminar shear box and compacted in 0.25 m-layers. The sand unit weight, γ, was 19.5 kN/m^3 and its average natural water content, w_c, was 5.5%. The sand bed was instrumented with accelerometers at various elevations on the east and west sides as well as in the center of the box. In addition, the laminar box was instrumented with accelerometers and Strain Potentiometers (SPs) at different elevations. More details about instrumentation and experimental setup are available in other studies (Elsawy et al. 2019a; Shahbazi et al. 2020).

Ten piles, including nine helical piles and one driven pile, were instrumented with strain gauges at different elevations and installed with a torque motor in the instrumented sand bed. Eight of the helical piles were installed in two groups of four piles (Shahbazi et al. 2020). In this study, only the piles that were tied together and formed group 1 (PG1) and group 2 (PG2) are discussed. Table 1 presents the piles dimensions and material properties. Pile 5 (3.66 m length, 88 mm diameter) was a driven pile, and pile 6 (3.66 m length, 76 mm side length) was a square single-helix pile. On TD4, each group of four-piles with similar diameters were connected to a steel skid filled with sand to simulate a superstructure inertial load. The 0.088 m-diameter piles were loaded with 62 kN and the 0.14 m-diameter piles were loaded with 98 kN. Accelerometers were placed on the outside of the skid at mid-height to record the acceleration of each skid. Fixed and pinned pile head connections were tested on TD4 and TD5, respectively. Figure 1 depicts the layout of piles while Fig. 2 presents the piles' instrumentation.

During all the testing days, the input motions followed the same order and magnitude. The first input motion each day consisted of white noise excitation (acceleration Root-Mean-Square (RMS) of 0.05 g) followed by scaled shakings of two replicated earthquake motions with known ground acceleration data; the 1994 Northridge California earthquake (Fire Station 108, 12,520 Mulholland Dr., USC station 5314, Component 35 degrees) and the 1995 Kobe earthquake (Takatori station, Component 0 degree). Both earthquakes are denoted herein as NOR and TAK respectively. These ground motions were applied at graduating intensities of 50%, 75% and 100% of the Peak Ground Acceleration (PGA) amplitude for both earthquakes. In addition, a low amplitude pulse wave was applied prior to each shaking and at the end of each testing day. Figure 3 presents a typical pulse wave and white noise signal as well as the

Table 1 Properties of test piles

Pile Group	Pile	Type*	Total Length/ depth (m)	Helix Level/helix diameter (m)	Outer Diameter/wall thickness (mm)	Yield strength (MPa)
PG1	P1	C–H	3.96/3.66	– 3.51/0.254	88/5.3	448.2
	P2	C–H	3.66/3.35	– 3.20/0.254		
	P3					
	P4	C–HH	3.66/3.35	– 2.59/0.254		
				– 3.20/0.203		
–	P5	C–D	3.66/3.35	–	88/5.3	448.2
	P6	S–H	3.66/3.35	– 3.20/0.254	76**/5.3	413.7
PG2	P7	C–H	4.22/3.35	– 3.20/0.254	140/10.5	551.6
	P8					
	P9					
	P10					

*C (circular), S (square), H (single helical pile), HH (double helical pile), D (driven pile)

**For square pile, 76 mm is the side length

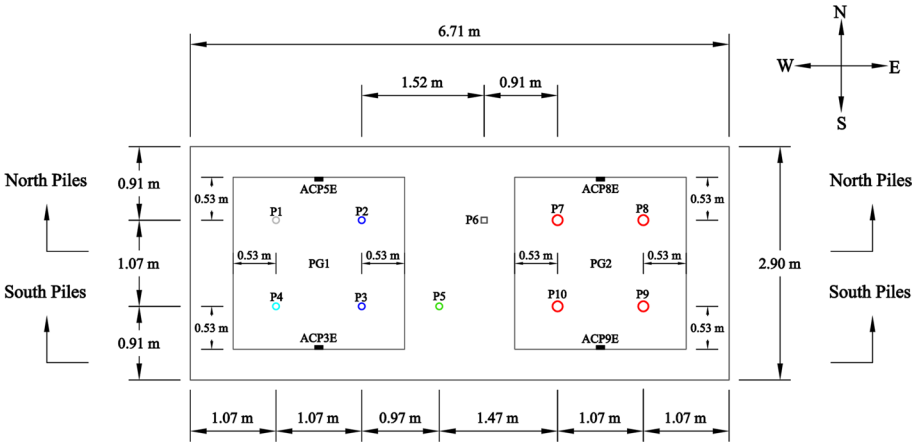

Fig. 1 Layout of test piles

unscaled earthquake records considered in the tests. It should be noted that these input motions were those recorded by the accelerometer located at the base of the shaking table.

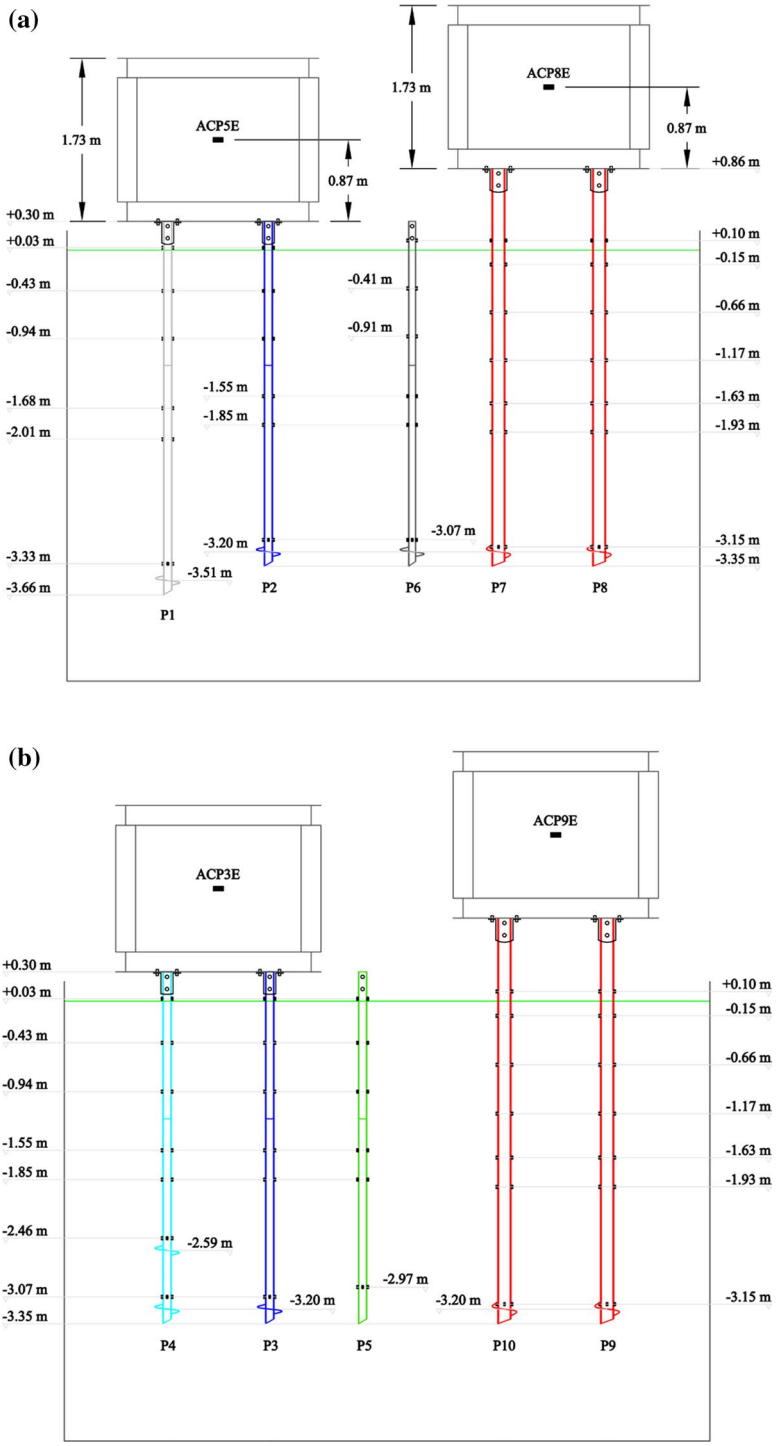

Fig. 2 Piles instrumentation: **a** North piles; **b** South piles

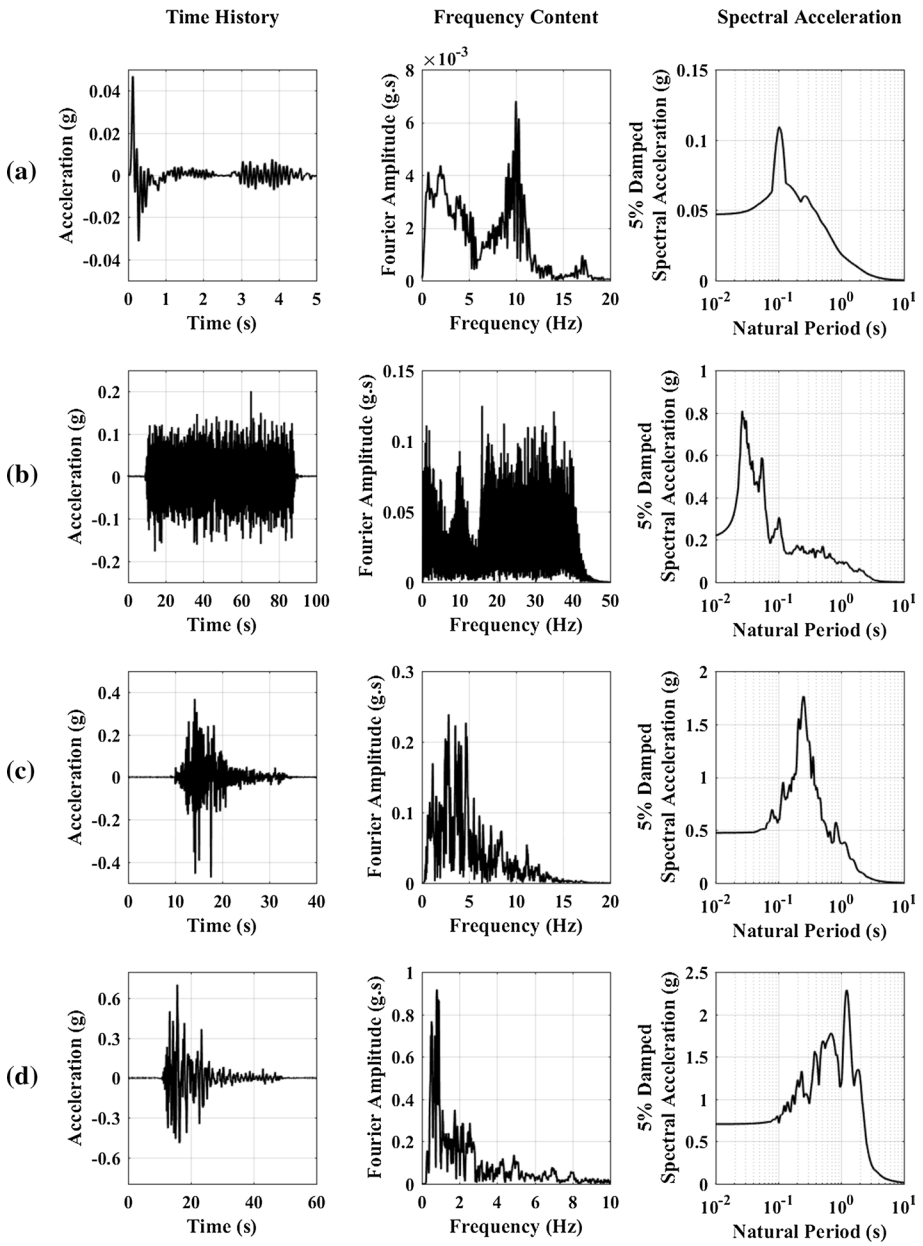

Fig. 3 Different properties of input motions considered in the testing program: **a** Pulse wave; **b** White noise signal; **c** NOR earthquake; **d** TAK earthquake

3 Dynamic properties of sand bed

3.1 Shear wave velocity

Pulse waves were applied prior to each shaking test and their measurements were used to calculate shear wave velocity of the sand bed. The shear wave velocity of each layer (i.e. between each two successive accelerometers) is calculated from:

$$v_{si} = \frac{h_u - h_l}{t_u - t_l} \tag{1}$$

where v_{si} is the shear wave velocity of layer i, h is the accelerometer elevation, t is the peak arrival time and subscripts u and l refer to the upper and lower accelerometers. Shear wave velocity profiles were constructed from the three accelerometer-arrays, east, center and west, and an average profile was computed. An example is presented in Fig. 4 for the first pulse on TD1. A weighted average for the shear wave velocity through the soil depth could be calculated from:

$$\bar{v}_s = \frac{H}{\sum_{i=1}^{n} \frac{h_i}{v_{si}}} \tag{2}$$

where H is the depth of sand bed, h_i and v_{si} are the height and shear wave velocity of each layer. The nth natural frequency of the sand bed can then be approximated by:

$$f_n = \frac{(2n-1) \times \bar{v}_s}{4 \times H} \tag{3}$$

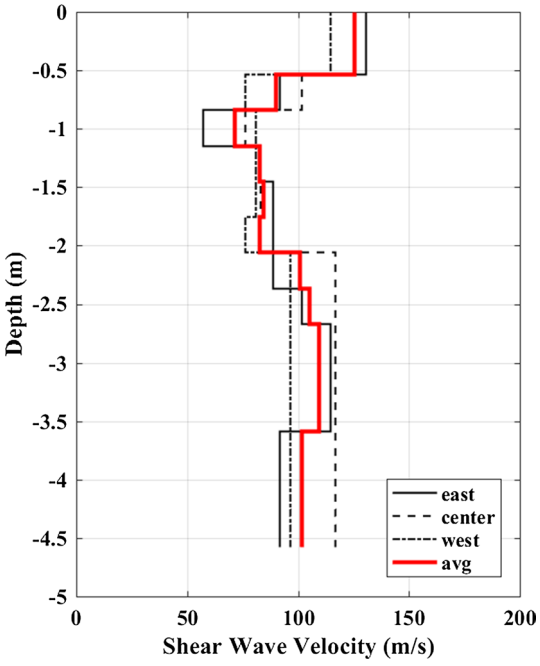

Fig. 4 Sand bed shear wave velocity profile on TD1

Throughout the experimental program, 39 pulses were applied to the test setup denoted Pulse (A) to Pulse (MM). The average shear wave velocity and corresponding fundamental frequency of the sand bed calculated from the responses to these pulses were found to be 100 m/s and 5.47 Hz, with slight changes through the testing program as can be seen from Fig. 5.

3.2 Shear strain

In addition to the shear wave velocity, the shear strain through the soil depth was determined from Strain Potentiometers (SPs) installed to the side of the shaking table, in which 15 of them were installed at different depths. These were used to record the time history of the soil block movement. It should be mentioned that the shear strain and damping ratio reported in this study are calculated from responses of the sand bed to pulse waves, which is a low amplitude excitation, in order to establish the dynamic properties of the sand bed at small strains. Damping ratios and corresponding soil shear strains due to large shakings were reported by Shahbazi et al. (2019).

A simple first order approximation was used to determine the shear strain between each two successive SPs from:

$$\gamma_i(t) = \frac{u_u(t) - u_l(t)}{z_u - z_l} \tag{4}$$

where γ_i is the shear strain in layer i, u is the displacement, z is the depth and subscripts u and l refer to the upper and lower SPs in the layer, respectively. Figure 6 presents the calculated absolute maximum shear strain in the soil depth from the first (Pulse A) and

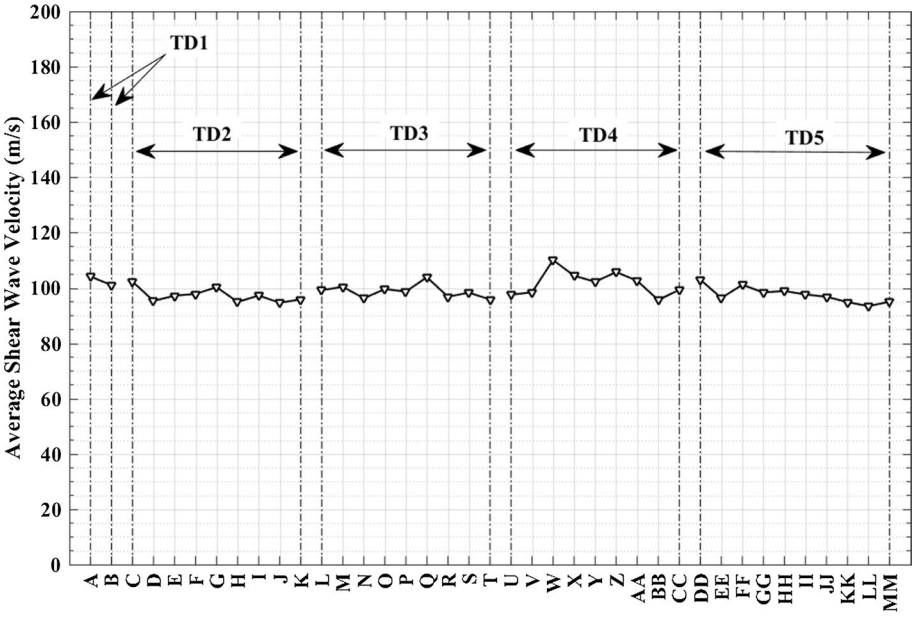

Fig. 5 Variation in sand bed's average shear wave velocity throughout the five testing days

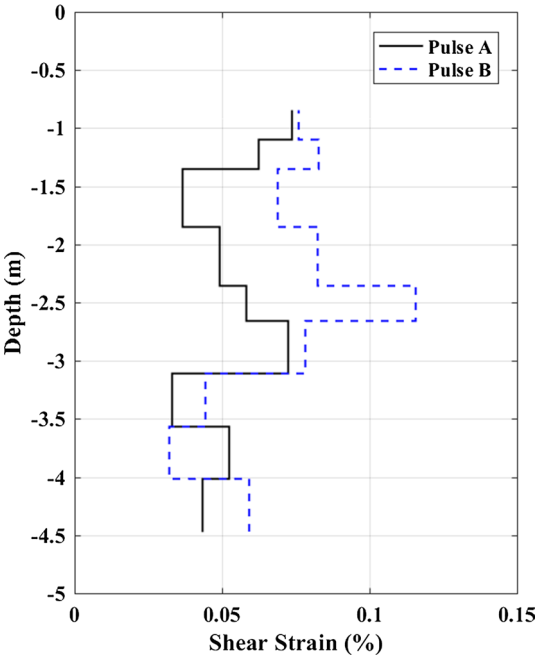

Fig. 6 Maximum absolute shear strain through soil depth at the beginning (Pulse A) and end (Pulse B) of TD1

last (Pulse B) pulses applied on TD1. As can be seen from Fig. 6, the shear strain did not show a clear trend throughout the soil depth. This could be attributed to non-uniformity in preparing the sand bed during the compaction process, especially closer to the laminar shear box borders, where the SPs used in the evaluation of the shear stress were installed. A very close trend was observed for the shear wave velocity as can be seen from Fig. 4. However, shear strains experienced by top soil layers were consistently larger because of the amplification of ground motion from bottom to top. The same observation was reported by Shahbazi et al. (2019). The weighted average maximum shear strain through the soil depth is calculated by:

$$\bar{\gamma} = \frac{H}{\sum_{i=1}^{n} \frac{h_i}{\gamma_i}} \tag{5}$$

where H is the total depth of the sand bed, h_i and γ_i are the height and shear strain of each layer, respectively. Table 2 provides a summary of maximum, minimum and average values

Table 2 Average soil shear strain and damping ratio during different testing days

Testing day	Shear Strain (%)			Damping Ratio
	Max	Min	Avg	Avg. (%)
TD1	0.0600	0.0574	0.0587	5.0
TD2	0.0602	0.0523	0.0558	5.0
TD3	0.0631	0.0503	0.0573	5.5
TD4	0.0721	0.0538	0.0614	11.0
TD5	0.0682	0.0513	0.0605	11.5

of shear strain experienced by the sand bed due to low amplitude pulse waves during each testing day. The soil shear strain varied slightly through the testing program.

3.3 Small strain damping ratio

The small strain damping ratio of the sand bed was evaluated from the responses time history of soil accelerometers to pulse waves. The logarithmic decrement method was used in which an exponential decrement curve was fitted to peaks of the response and an appropriate number of cycles was considered as recommended by Tweten et al. (2014). The appropriate number of cycles was 9 for the measurements taken on TD4 and TD5. The logarithmic decrement was calculated between each two peaks through the number of cycles in the range considered and the damping ratio was taken as the average value. The damping ratio profile through the soil depth was calculated from the three accelerometer-arrays and an average profile was constructed. The average value of damping ratio through soil depth was determined for each testing day and the results are presented in Table 2.

It is noted that the soil damping ratio in the first 2 days was small because there was no inertial loading. Inertial masses were placed on pile heads in TD3, and the damping ratio increased by 10% due to the increase in the response of pile-soil systems associated with inertial forces. A substantial increase in the damping ratio occurred in TD4 and TD5 when pile groups were tested. This was due to the large weights of the pile caps, and the corresponding increase in soil response especially in the soil enclosed within the pile groups. The values of damping ratio are compared to the damping curves provided by Seed and Idriss (1970) in Fig. 7. As noted in Fig. 7, the calculated damping ratios fall within the

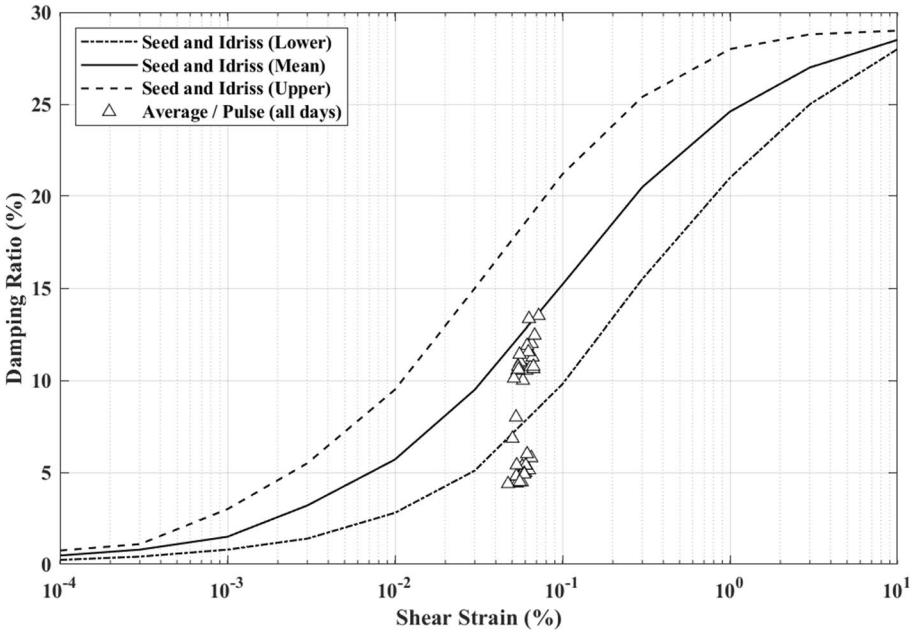

Fig. 7 Comparison of damping ratio with Seed and Idriss (1970) damping curves

minimum (TD1, TD2 and TD3) and mean (TD4 and TD5) damping curves suggested by Seed an Idriss (1970).

4 Natural frequency

Response of pile-soil system to dynamic loads is mainly influenced by its natural frequency, in which significantly larger responses would be expected whenever the natural frequency is matching, or close to, either the predominant frequency of the earthquake and/or the natural frequency of the surrounding soil medium.

Natural frequencies of a pile-soil system can be obtained by subjecting the system to a sweep of harmonic loads with varying frequencies and observing the frequencies associated with peaks of the response, which correspond to the system's natural frequencies. Alternatively, the natural frequency of a system can be determined from the response time history of the system subjected to a transient dynamic load. In that case, natural frequencies could be determined through transferring the response time history to the frequency domain employing a Fast Fourier Transform (FFT) algorithm.

The FFT analysis can be used to evaluate the system's natural frequencies accurately and clearly if the input signal has uniform and nearly constant amplitude for the range of frequencies under consideration, i.e., an ideal white noise signal. However, typical transient loading would have a wide range of frequencies with varying amplitudes. In such case, the response amplitudes at different frequencies should be compared with the input amplitudes at the same frequencies to determine locations of the peaks where maximum amplifications of the input signal occur. However, it can be difficult to establish the peaks and there would be some spurious peaks, especially at higher modes of vibration. The FFT comprises fewer steps and can provide a fast estimate of the fundamental natural frequency; however, it may not be accurate. Therefore, the FFT method is not recommended if higher modes of vibration are to be considered.

On the other hand, natural frequencies could also be evaluated from the Frequency Response Function (FRF), defined as the ratio between the response frequency amplitude to the input frequency amplitude. The FRF method yields a smooth curve with distinct peaks at frequencies that correspond to the natural frequencies of the system. It can also provide good results regardless of the input signal, i.e. it does not require a perfect white noise input signal. It is recommended to employ the FRF method to evaluate the natural frequencies of the system, as it is more accurate, especially for higher modes of vibration. Another advantage of the FRF is that it gives an indication of the amplification of the input ground motion.

The white noise signal employed in the experimental program did not have a constant frequency amplitude as can be seen from Fig. 3b. Hence, differences between the values of natural frequencies obtained from FFT and FRF for different systems were expected as would be shown in later sections.

Responses due to white noise signals were utilized in both methods. To evaluate the natural frequencies of the sand bed, responses of soil accelerometers were used. On the other hand, to assess the natural frequencies of single piles and pile groups, responses of pile accelerometers as well as strain gauges were utilized. It should be noted that white noise signals were applied only once at the beginning of each testing day; thus it provided one estimate for the natural frequency for each day representing soil and/or piles configurations

during the five testing days. Alternatively, natural frequencies were also evaluated from the response to pulse waves in order to evaluate the effect of successive shakings.

4.1 Sand bed

Separating the natural frequencies of the pile foundation and the surrounding soil with an acceptable margin ensures the foundation response is not adversely affected by the resonance condition, which could lead to large deformations and straining actions in the piles. Hence, it is essential to accurately determine different natural frequencies of the soil corresponding to different modes of vibration.

An example of the frequency response of the east array of accelerometers due to white noise signal applied on TD1 is shown in Fig. 8. It is noted from Fig. 8 that the values of natural frequencies evaluated from the FFT and FRF methods differ by 10% approximately. It is also noted that higher vibration modes are more pronounced from the measurements of lower accelerometers. This is because the soil box experienced more rotation at the bottom near its connection to the shake table, while the top of sand bed experienced less rotation but larger horizontal movement. Thus, the fundamental (horizontal) natural frequency was evaluated from the measurements of the top accelerometer, while higher modes were evaluated from the measurements of lower accelerometers. Finally, the FRF method provided a more identifiable second natural frequency compared to the FFT method, especially in top accelerometer.

The natural frequency was computed from the three accelerometer-arrays, and an average value was considered. Figure 9 compares the responses of the top accelerometer of

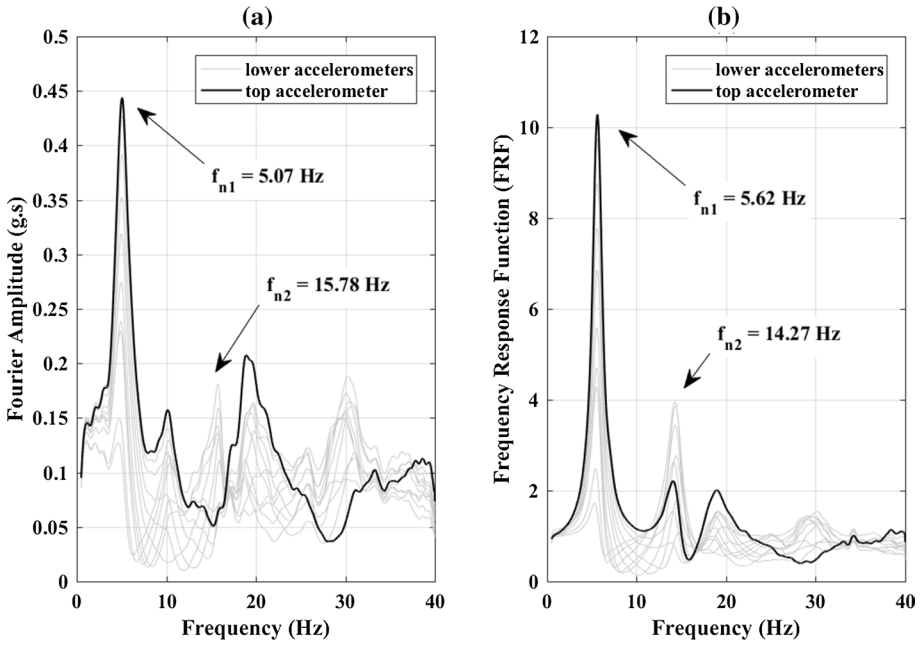

Fig. 8 Frequency response of the east array of accelerometers due to white noise signal on TD1: **a** FFT; **b** FRF

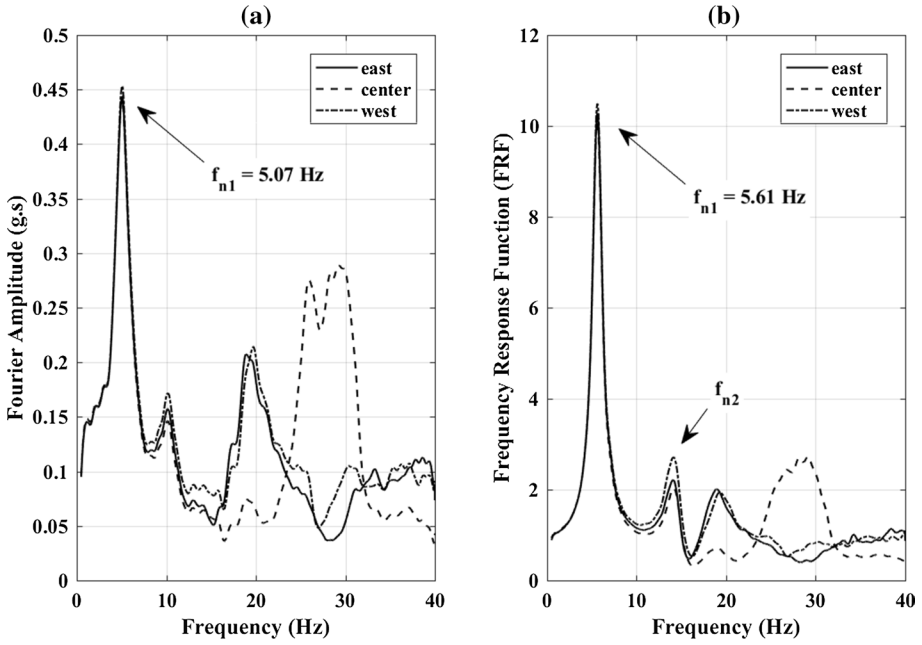

Fig. 9 Frequency response of the top accelerometer in east, center and west arrays due to white noise signal on TD1: **a** FFT; **b** FRF

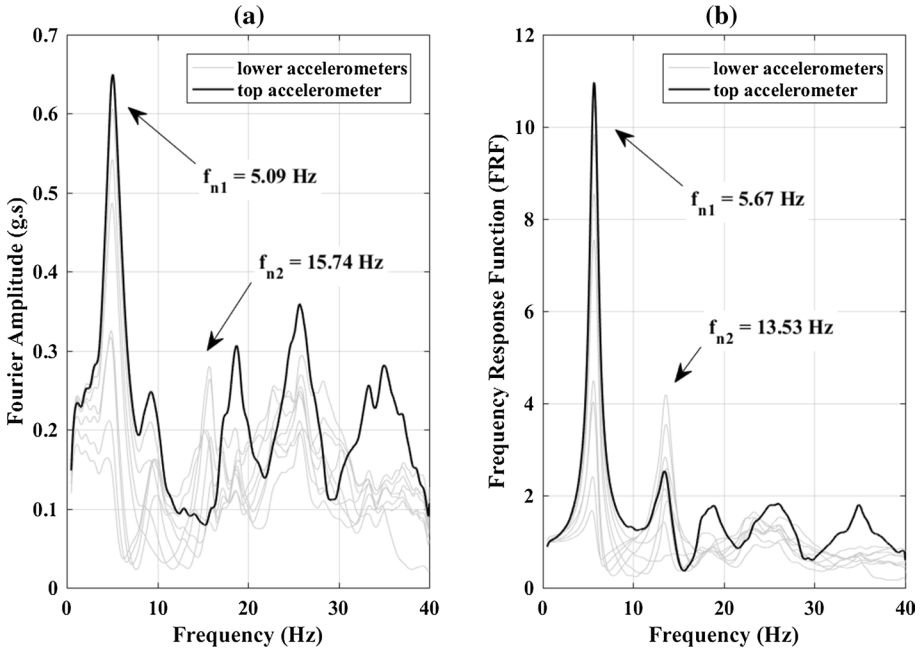

Fig. 10 Frequency response of the east array of accelerometers due to white noise signal on TD2: **a** FFT; **b** FRF

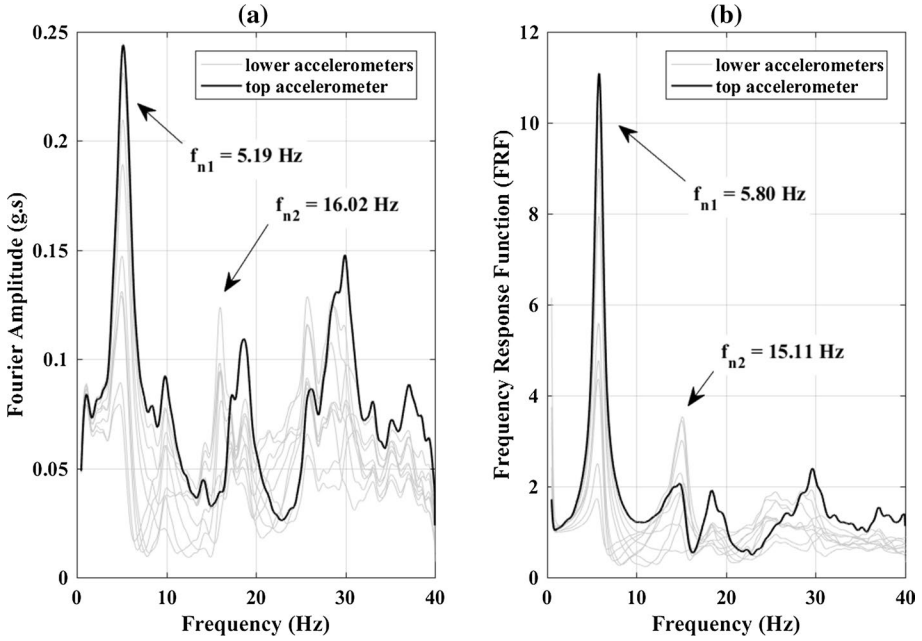

Fig. 11 Frequency response of the east array of accelerometers due to white noise signal on TD3: **a** FFT; **b** FRF

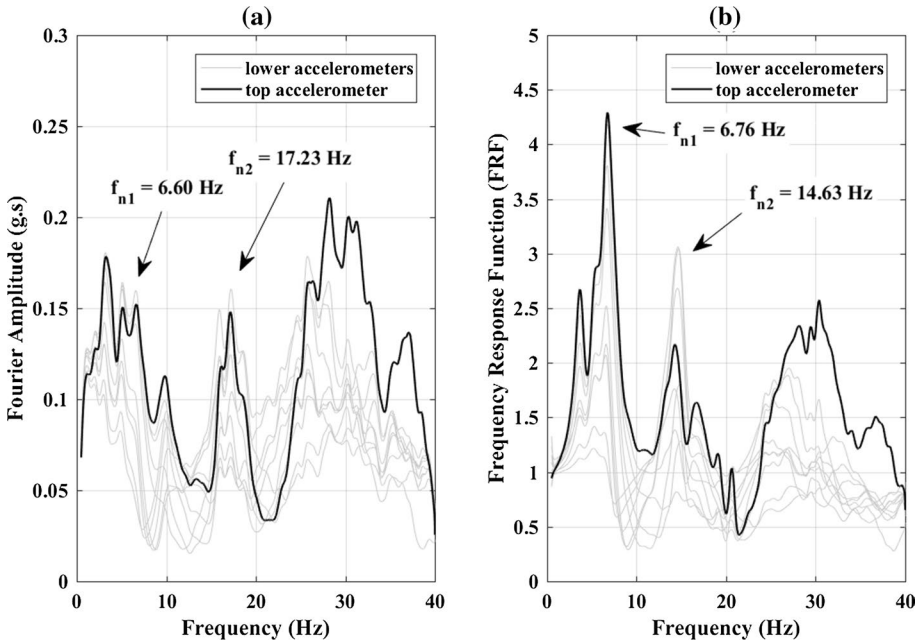

Fig. 12 Frequency response of the east array of accelerometers due to white noise signal on TD4: **a** FFT; **b** FRF

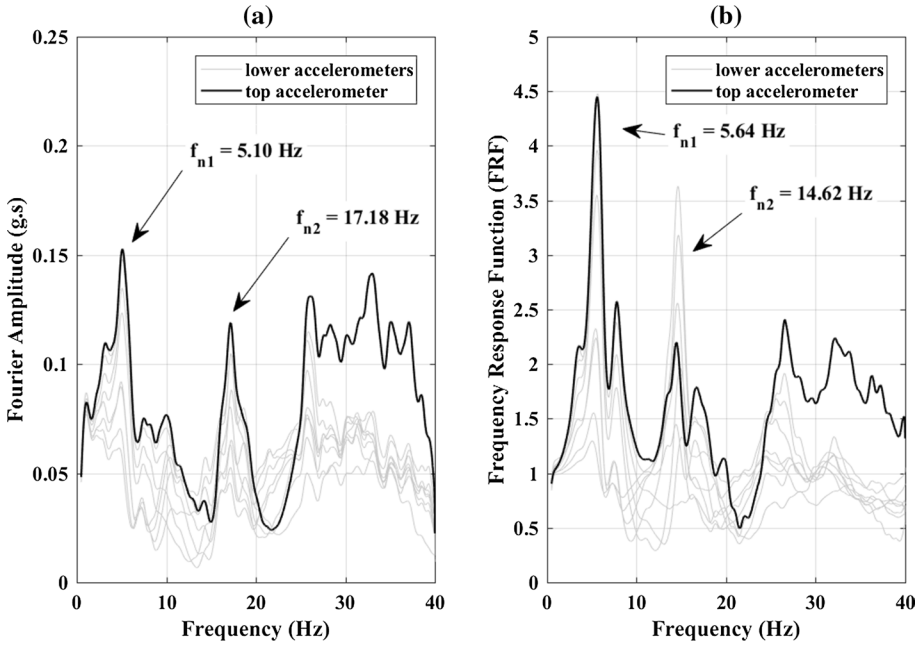

Fig. 13 Frequency response of the east array of accelerometers due to white noise signal on TD5: **a** FFT; **b** FRF

the three arrays on TD1, which shows an excellent agreement in both the first and second natural frequencies.

Figures 10, 11, 12 and 13 present the soil frequency response obtained from the east array of accelerometers in TD2 to TD5, respectively. These figures indicate the effects of the installed piles in TD2, adding the inertial masses in TD3 and adding the model structure in TD4 and TD5. The soil Fourier spectra displayed more peaks due to the interaction with the piles and the influence of their natural frequencies. This is particularly evident on TD4 and TD5 where it is difficult to differentiate between peaks corresponding to different natural frequencies of the surrounding sand bed and those corresponding to different pile group-soil systems. For example, Fig. 12 shows that the effect of PG2 response on the FFT spectra was even larger than that of the soil itself; the maximum peak is observed at around 4 Hz, which corresponds to the natural frequency of PG2. Given the multiple peaks exhibited by the FFT, the FRF results were obtained first and then the value of the nearest

Table 3 First natural frequency of the sand bed

Testing day		TD1	TD2	TD3	TD4	TD5
Average FFT Amplitude (g.s)	Input	0.035	0.047	0.023	0.038	0.031
	Response	0.354	0.507	0.255	0.168	0.144
Response Amplification (%)		1028	1087	1098	444	497
f_{n1} (Hz)	FFT	5.07	5.09	5.19	6.60	5.12
	FRF	5.61	5.67	5.80	6.74	5.64

Table 4 Second natural frequency of the sand bed

Testing day		TD1	TD2	TD3	TD4	TD5
Fourier Amplitude (g.s)	Input	0.033	0.034	0.021	0.027	0.017
	Response	0.110	0.128	0.067	0.074	0.055
Response Amplification (%)		358	383	324	284	334
f_{n2} (Hz)	FFT	15.78	15.69	16.03	17.23	17.21
	FRF	14.26	13.59	15.10	14.63	14.68

peak from FFT was evaluated. The difference between the natural frequencies of the second mode of vibration evaluated from the FFT and FRF results on TD4 and TD5 was about 20%.

A summary of the first and second natural frequencies of the sand bed throughout the five testing days as well as Fourier amplitudes of the input and response and the amplification ratio are shown in Tables 3 and 4, respectively, from the FFT and FRF methods.

4.1.1 Effect of successive shaking

In order to evaluate the effect of successive shaking on the natural frequency of the system, pulse waves were used. The pulse wave measurements could only be used to evaluate the first natural frequency because the second natural frequency was outside its frequency range. The results obtained from the FRF for all pulse waves and white noise signals are plotted in Fig. 14. The approximate values of the natural frequency obtained from shear

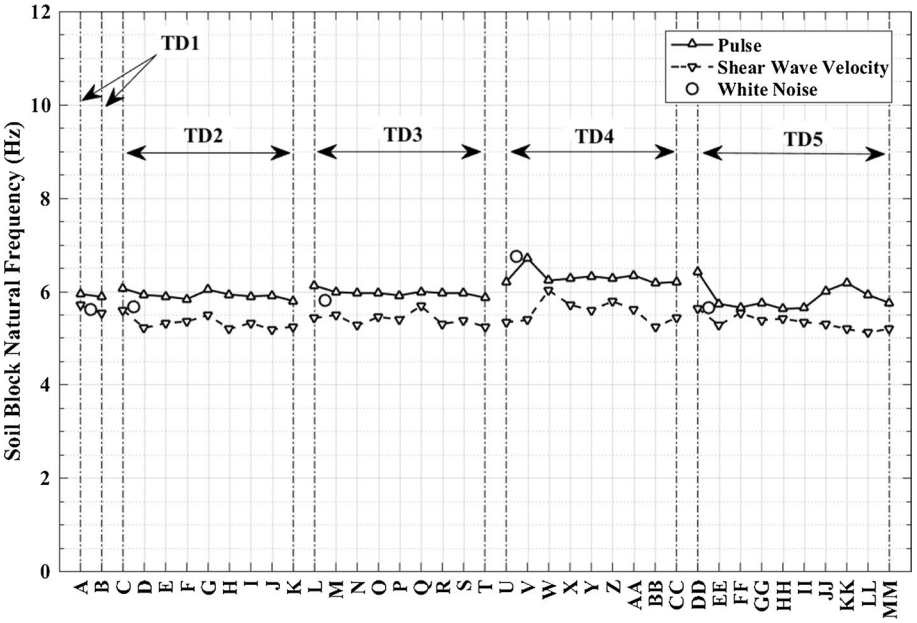

Fig. 14 Variation in the natural frequency of the sand bed throughout the testing program

wave velocity using Eq. 3 are plotted as well. It is observed from Fig. 14 that the sand bed's fundamental frequency remained nearly constant throughout the testing program. This means that successive shaking had negligible effect on the soil's natural frequency, i.e., no degradation of the soil stiffness. It is also noted that the natural frequency values calculated from pulse waves responses were higher than the values evaluated from the measured shear wave velocity.

4.2 Single piles with no head masses

Natural frequencies of single piles were evaluated employing their responses to white noise signals. On the other hand, pulse waves responses were used to explore the effect of successive shaking. The responses recorded from pile accelerometers and strain gauges were analyzed and compared. Since, the focus of this study is on pile groups, only the results of piles (P1–P4) and (P7–P10) are presented herein.

Piles were installed in TD2 with no head masses. This means only kinematic interaction occurred between piles and the soil during the shaking, and piles responses are influenced by the vibration of the sand bed and its natural frequencies.

As an example, Fig. 15 presents the FRF of pile P10 to the white noise signal. Figure 15 shows response peaks corresponding to the natural frequencies of the soil's vibration modes. Moreover, responses from both accelerometer and strain gauges coincide; however, peaks at higher modes were more pronounced in the accelerometer response. This is attributed to the large rotation that occurred at the location of the accelerometer at the pile head, while the strain gauge was located at the ground surface. Table 5 presents the piles'

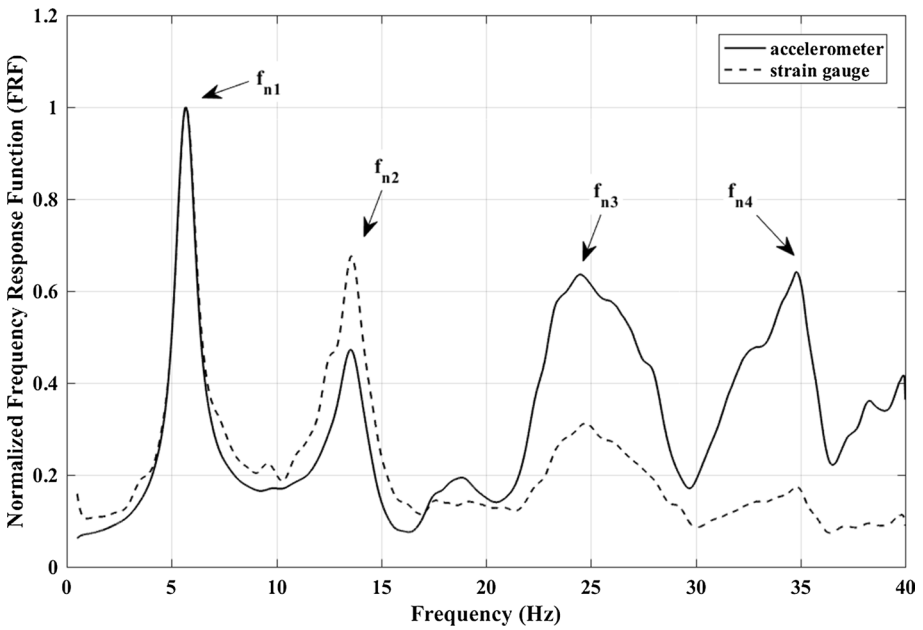

Fig. 15 FRF of P10 due to white noise signal on TD2

Table 5 Fundamental frequency of piles during TD2

f_{n1} (Hz)	Accelerometer		Strain Gauge	
	FFT	FRF	FFT	FRF
P1	–	–	5.21	5.69
P2	5.09	5.67	5.26	5.68
P3	5.12	5.68	5.07	5.69
P4	5.12	5.68	5.11	5.70
P7	5.11	5.68	5.13	5.71
P8	5.12	5.68	5.15	5.69
P9	5.14	5.68	5.11	5.70
P10	5.14	5.68	5.03	5.65

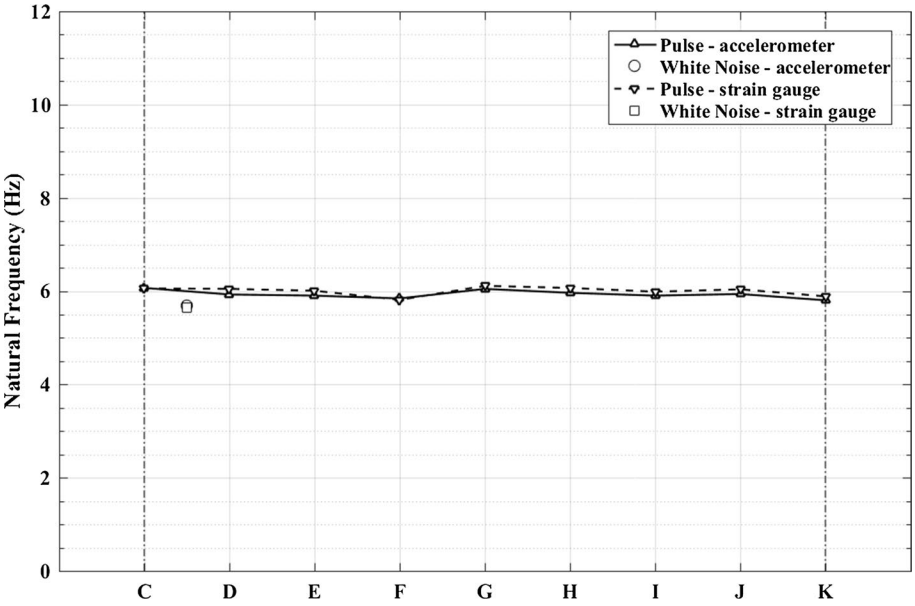

Fig. 16 Variation in the fundamental natural frequency of P10 during TD2

first natural frequencies evaluated from the white noise signal for both accelerometers and strain gauges.

4.2.1 Effect of successive shaking

Responses of single piles to pulse waves were used to evaluate the effect of successive shaking on the fundamental frequency. Figure 16 displays the variation of the fundamental frequency of pile P10 evaluated from FRF throughout TD2 (Pulse (C) to Pulse (K)). It can be seen from Fig. 14 that the natural frequency remained almost constant

throughout all pulses and that values obtained from accelerometers and strain gauges were almost identical. It is noted that the pile's natural frequency matched that of the sand bed. Similar results were obtained for all piles (P1–P4) and (P7–P10).

4.3 Single piles with head masses

Different masses were placed on top of piles in TD3. Thus, both inertial and kinematic soil-pile interaction took place and influenced the response of the pile-soil systems. This was manifested in the soil vibration at a frequency close to the natural frequency of piles.

The pile responses to white noise signal recorded by accelerometer and strain gauges were analyzed to evaluate the natural frequencies. For example, Fig. 17 shows the responses of pile P4. The following observations can be made from Fig. 15. The pile's response exhibited peaks corresponding to the first and second natural frequencies of the sand bed due to the interaction between the soil and the pile. The fundamental frequencies obtained from accelerometer and strain gauges coincided; however, the spectral amplitudes at these frequencies were higher in the strain gauge response. It is also noted that the pile's response was dominated by the horizontal vibration mode because its second natural frequency was outside the frequency content of the white noise signal (i.e. 0–40 Hz).

4.3.1 Effect of pile's geometric properties on its natural frequency

Responses measured by strain gauges were utilized to investigate the effect of different pile's gemoetric properties on its natural frequency as they featured clear peaks and were

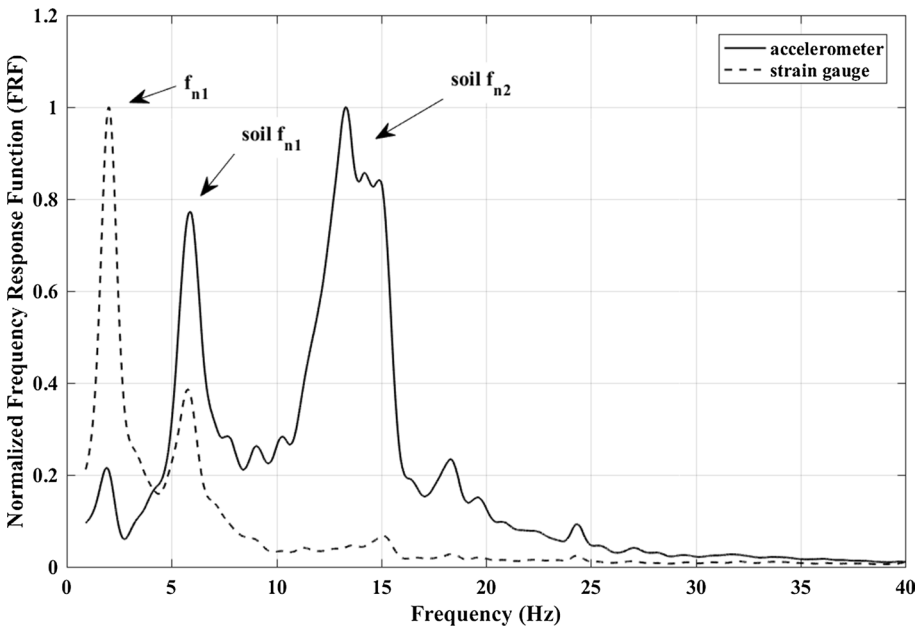

Fig. 17 Normalized FRF of P4 due to white noise signal on TD3

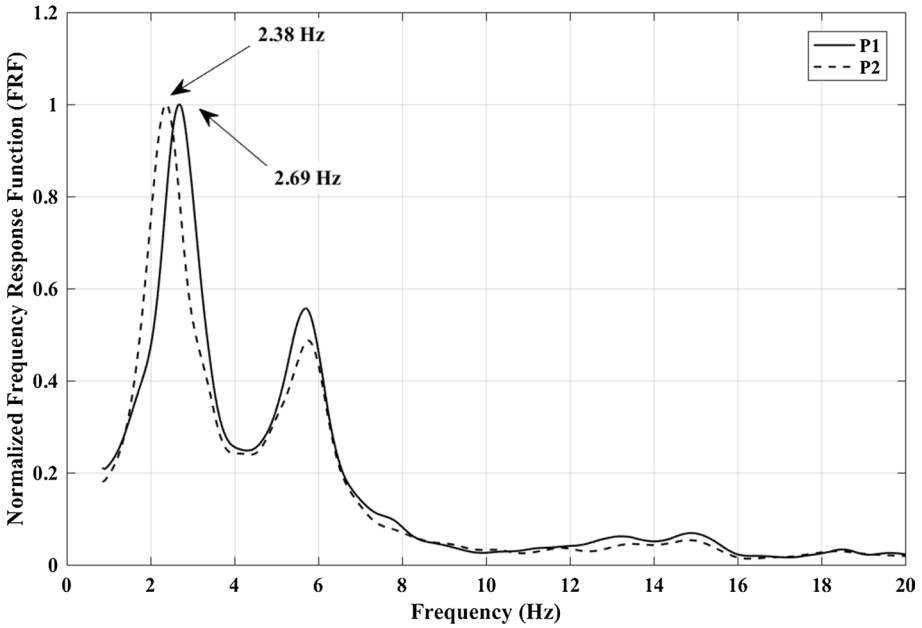

Fig. 18 Normalized FRF for P1 and P2 due to white noise signal on TD3

less affected by the soil's vibration. However, natural frequency values from both accelerometers and strain gauges were close.

4.3.1.1 Effect of pile's embedment depth The pile's embedment depth affects its natural frequency. It is expected that increasing the embedment depth would increase the stiffness and hence the natural frequency. This effect is explored by comparing the natural frequencies of P1 (3.66 m) and P2 (3.35 m). Figure 18 shows that even though P1 had slightly larger pile head mass (768 kg) than P2 (749 kg), its natural frequency was greater than that of P2.

4.3.1.2 Effect of number of helices To evaluate the effect of the number of helices on the pile's natural frequency, responses of P2 and P4 are compared. Both piles had the same cross-section and pile head mass but P4 had two helices and P2 had one helix. As seen in Fig. 19, P4 had slightly lower natural frequency than P2. This is attributed to the additional disturbance of soil along the pile shaft owing to the passage of two helices for P4, hence reducing the stiffness of pile-soil system. Elsherbiny et al. (2017) reported similar observation from full scale testing of helical piles installed in dense sand and subjected to harmonic loading. It should be noted that the second helix was well below the effective depth for lateral resistance; thus, it did not contribute to the lateral stiffness of the pile.

4.3.1.3 Effect of pile's free (stick-out) length The free (stick-out) length of the pile is defined as the distance from the ground surface to the center of gravity of the pile-head mass. To determine the effect of the pile's free length on its natural frequency, the natural frequencies of P7 and P8 that had the same cross-section but different free length (1.72 m and 1.45 m

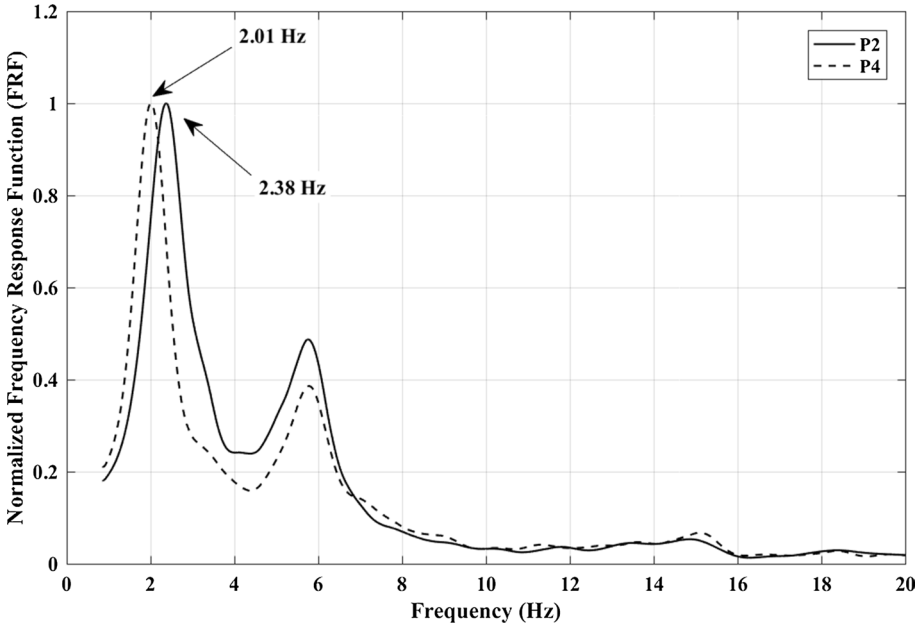

Fig. 19 Normalized FRF for P2 and P4 due to white noise signal on TD3

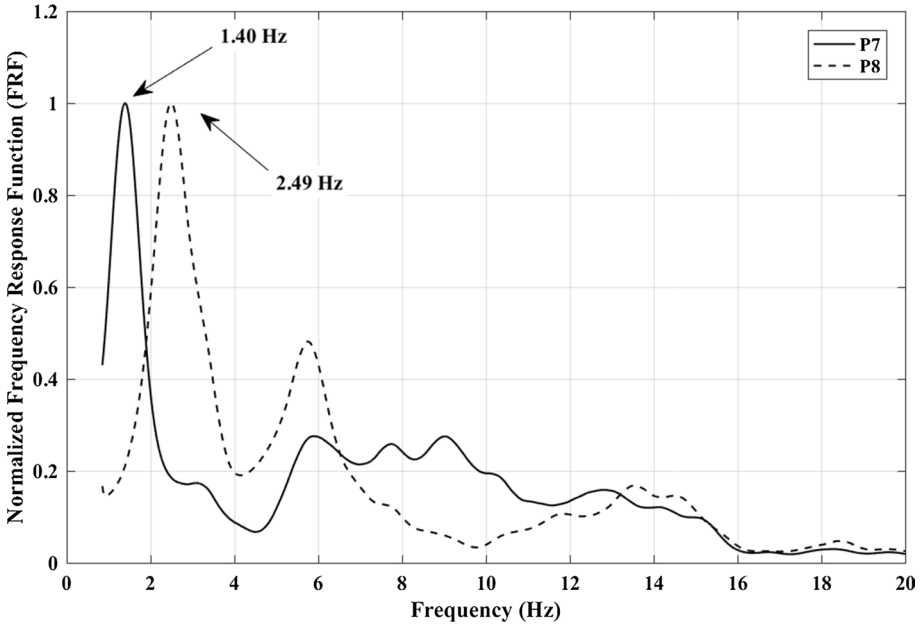

Fig. 20 Normalized FRF for P7 and P8 due to white noise signal on TD3

for P7 and P8, respectively) are compared. As shown in Fig. 20, the natural frequencies for P7 and P8 were 1.4 Hz and 2.49 Hz, respectively. The head mass for P7 was 1236 kg and the head mass for P8 was 785 kg. In order to isolate the effect of free length, the natural frequency of P8 was adjusted considering the same mass as P7. The natural frequency, f_n, of any system is given by:

$$f_n = \frac{1}{2\pi}\sqrt{\frac{k}{m}} \tag{6}$$

where k and m are stiffness and mass, respectively. Using Eq. 6, the stiffness of P8 was determined, then its natural frequency was calculated considering a head mass of 1236 kg (same as P7), which yielded a natural frequency of 1.98 Hz. This large difference in natural frequency (1.98 Hz compared to 1.40 Hz) clearly demonstrates the significant impact of the pile's free length on its lateral stiffness and natural frequency. This should be an important consideration in design of piles subjected to dynamic lateral loads.

4.3.1.4 Effect of pile's flexural rigidity To evaluate the effect of pile's flexural rigidity (stiffness) on its natural frequency, piles of different cross-sections are considered. However, the two piles that had different cross-sections (88 mm and 140 mm) had different masses and free lengths as well. Thus, it was not possible to isolate the effect of the flexural stiffness, rather a combined effect of all three parameters could be evaluated.

Figure 21 presents the responses of piles P2, P8 and P10. P8 and P2 had pile head masses of 785 kg and 749 kg, and free lengths of 1.45 m and 0.86 m, respectively. The natural frequency of P8 was adjusted using Eq. 6 to consider the same mass as P2. The

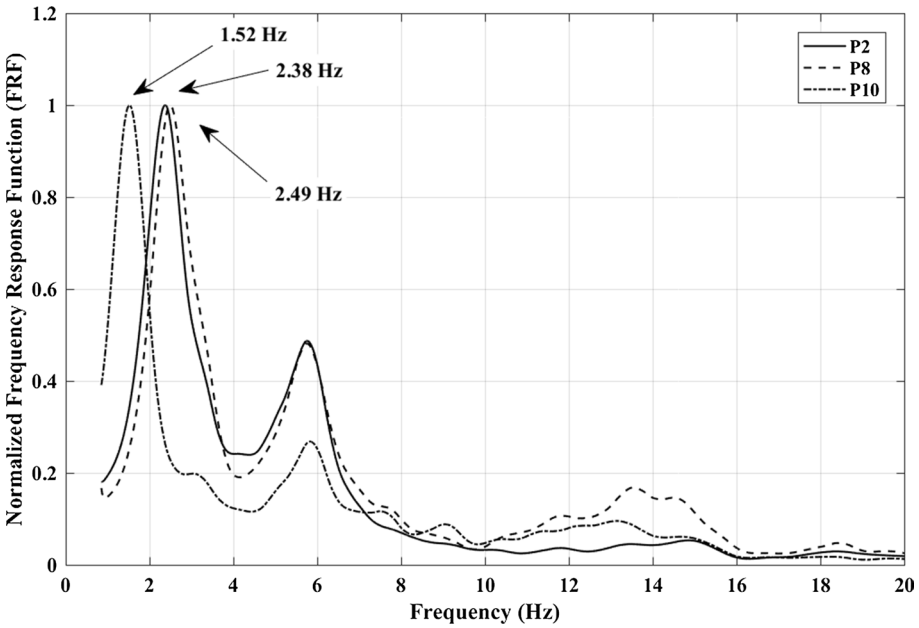

Fig. 21 Normalized FRF for P2, P8 and P10 due to white noise signal on TD3

natural frequency of P2 was 2.38 Hz and the adjusted natural frequency of P8 was 2.55 Hz, which indicates that the increase in the stiffness of P8 due to its larger cross-section was more than the decrease due to the given larger free length. Meanwhile, head mass of P10 was 1244 kg and its free length was 1.74 m. Its adjusted natural frequency considering head mass equal to that of P2 was 1.96 Hz. In that case, the much larger free length of P10 (1.74 m compared to 0.86 m for P2) resulted in a substantial reduction in its natural frequency regardless of its larger cross-section.

4.3.2 Summary of natural frequencies of single piles

The natural frequencies computed from FFT and FRF varied slightly. On the other hand, the results from strain gauges and accelerometers were in good agreement, with the values from strain gauge responses slightly higher than those obtained from accelerometer responses. Table 6 summarizes the natural frequencies for piles P1–P4 and P7–P10. It is noted from Table 6 that all piles had natural frequencies in the range of 1–3 Hz, which is closer to the predominant frequency of TAK earthquake than that of the NOR earthquake. Therefore, the resonance effects would be expected to be higher, and consequently higher pile responses for the TAK earthquake. This is manifested in the spectral accelerations for each earthquake presented in Table 6.

4.3.3 Effect of successive shakings

Piles responses to pulse waves were utilized to evaluate the effect of successive shakings on their fundamental frequencies. The natural frequencies obtained from measurements of accelerometers were slightly lower than those obtained from strain gauges measurement but exhibited the same trends. Therefore, only the natural frequencies obtained from strain gauge measurements for piles P1, P2, P4, P8 and P10 on TD3 (Pulse (L) to Pulse (T)) are shown in Fig. 22. Generally, the natural frequencies decreased through successive shakings as expected, which is attributed to multiple reasons. First, degradation in the pile-soil stiffness due to the significant nonlinearity experienced by the soil adjacent to the pile shaft (especially the top portion) associated with gap opening then sand cave-in to fill the gap, which resulted in loosening the soil around the piles and hence a reduction in the soil's stiffness. Second, the formation of gaps around the pile shaft at the top portion increased

Table 6 Natural periods and expected spectral accelerations for piles in TD3

Pile	Fundamental frequency (Hz)	Fundamental period (s)	Expected spectral acceleration for NOR earthquake (g)	Expected spectral acceleration for TAK earthquake (g)
P1	2.69	0.372	0.98	1.52
P2	2.38	0.420	0.87	1.41
P3	1.84	0.543	0.57	1.64
P4	2.01	0.498	0.59	1.66
P7	1.40	0.714	0.38	1.76
P8	2.49	0.402	0.88	1.53
P9	2.99	0.334	1.00	1.13
P10	1.52	0.658	0.49	1.75

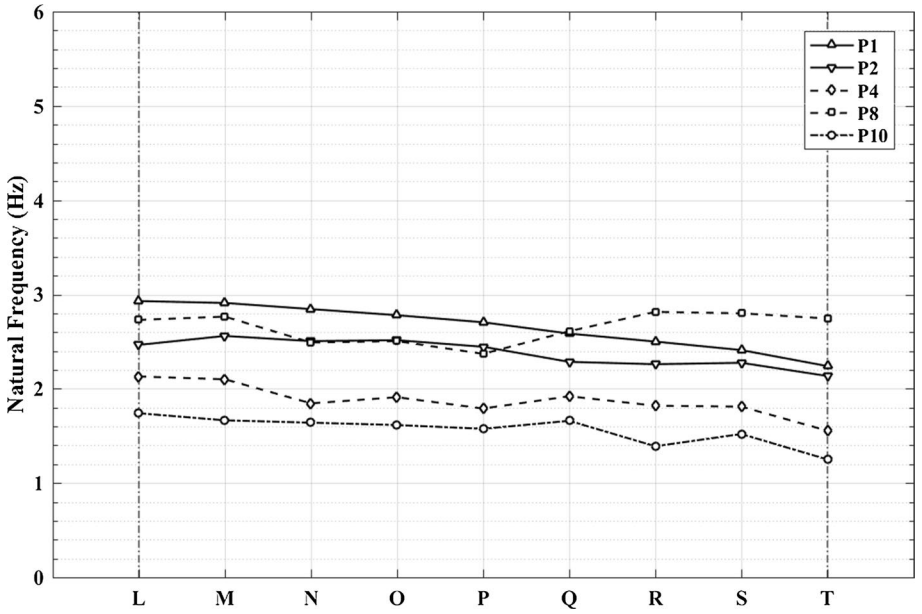

Fig. 22 Variation in the fundamental frequency of P1, P2, P4, P8 and P10 with successive shakings during TD3

the free length of the pile and in turn reduced its natural frequency. Finally, as the soil became softer, the volume of soil vibrating with the pile increased, which could further decrease the natural frequency. However, the natural frequency of some piles remained constant or even increased through successive shakings. This is attributed to closure of gaps around pile shaft and hence increased stiffness of the pile-soil system. The gap opening and closure was confirmed by visual observations during the tests (through video camera recordings).

4.3.4 Analytical model

Several approaches are employed to analyze the Soil-Structure Interaction (SSI) and dynamic response of piles (El Naggar 2004). These approaches include: continuum methods, Boundary Element Methods (BEM), dynamic Beam on Nonlinear Winkler Foundation (BNWF), and Finite-Element Models (FEM).

The continuum approach is generally rigorous, and its solution can be formulated in closed form equations to reduce the computational effort. Novak (1974) and Novak and Aboul-Ella (1978) developed closed-form formulas to determine the complex impedance of single and grouped piles assuming linear visco-elastic behaviour of the pile and soil. Kaynia (1982) and Kaynia and Kausel (1982) have presented closed form solutions based on Green's functions incorporated in the Boundary Element Method to determine the dynamic stiffness of pile groups.

In BNWF models, the pile is simulated as a series of discrete linear elastic beam-column elements and the surrounding soil is modeled by a series of non-linear detachable Winkler springs and dashpots on each side of the pile to represent the soil's stiffness and damping

(El Naggar and Novak 1994, 1995; Boulanger et al. 1999; Mostafa and El Naggar 2002; El Naggar et al. 2005). Owing to its simplicity, the BNWF approach is widely employed; however, coupling effects between different layers along the piles are not accounted for. It can be particularly efficient for modeling pile and soil nonlinearity, gapping between pile and soil as well as degradation of soil's strength and stiffness (Allotey and El Naggar 2008; Heidari et al. 2014).

The Finite Element method (FEM) is a versatile approach, which is widely used for SSI problems. It can simulate the behavior of soil and structures with complex geometry subjected to varying loading conditions (Seed and Lysmer 1978; Maheshwari et al. 2004, 2005; Lou et al. 2011; Stewart et al. 2012; Elsharnouby and El Naggar 2018b). FEM can be employed to simulate the nonlinear seismic response of piles embedded in layered soil considering different aspects of pile–soil interaction; however, it can be computationally very demanding.

The computer software DYNA6 (El Naggar et al. 2011) is used to evaluate the dynamic characteristics and responses of different types of foundations subjected to harmonic, transient or random loads. It evaluates the dynamic characteristics of single piles employing the plane strain solutions proposed by Novak (1974). The pile group's stiffness and damping constants are then evaluated employing the superposition approach proposed by El Naggar and Novak (1994, 1995), which utilizes the interaction factors proposed by Kaynia and Kausel (1982). This approach can simulate piles with varying cross-section (to account for the helices), variation of soil properties along the pile shaft, and the pile and head fixity conditions as well as the geometrical properties and mass of the structure placed on the pile head. DYNA6 can also approximate the gap opening and the degradation of soil stiffness within the annular zone around the pile shaft (Elkasabgy and El Naggar 2018).

The program DYNA6 is employed in this study to evaluate the dynamic characteristics of the test single piles. Two models were constructed, one for the 88 mm-diameter pile and one for the 140 mm diameter pile. The soil profile was modeled as a homogenous layer with the measured soil properties from the experimental program, i.e., shear wave velocity, $V_s = 100$ m/s, damping ratio, $D = 0.05$, Poisson's ratio, $\nu_s = 0.3$ and unit weight, $\gamma_s = 19.5$ kN/m^3. To model the free length of the pile (length from the ground surface to the bottom of the pile cap), a soil layer with the same depth was defined and assigned zero stiffness (i.e., shear wave velocity = 0.0 m/s). Piles were modeled as steel pipes with their corresponding lengths and inner and outer diameters. The helices were idealized as plates with the same thickness and modeled in the mid-height of the pitch. The pile's material was modeled as linear with Young's Modulus, $E_p = 200$ GPa, Poisson's ratio, $\nu_p = 0.3$, damping ratio, $D_p = 0.02$ and unit weight, $\gamma_p = 77$ kN/m^3. The piles were considered as end bearing with a fixed pile head. The pile caps were modeled as cylinders with the corresponding dimensions and density as the actual mass used in the tests.

A harmonic loading scheme was employed in which a sweep of harmonic loads with frequencies ranging from 0.05 to 40 Hz with 0.05 Hz step were applied to the pile-soil system and the corresponding response at the center of gravity of the pile mass was calculated. The natural frequency corresponded to the frequency at which the maximum response was calculated. Figures 23 and 24 compare the natural frequencies calculated using DYNA6 with those evaluated from the experimental results on TD3 (Pulse (L) to Pulse (T)) for piles P1 and P10, respectively.

Figures 23 and 24 display the results from different analyses that were performed to capture the correct dynamic characteristics of the test piles. The initial analysis was performed considering the pile cap dimensions, pile cap mass and free length of the pile as well as the helix properties and considering the measured soil properties along the embedded length of the pile. The results from this analysis are denoted (DYNA6—no gap—no weak zone). As

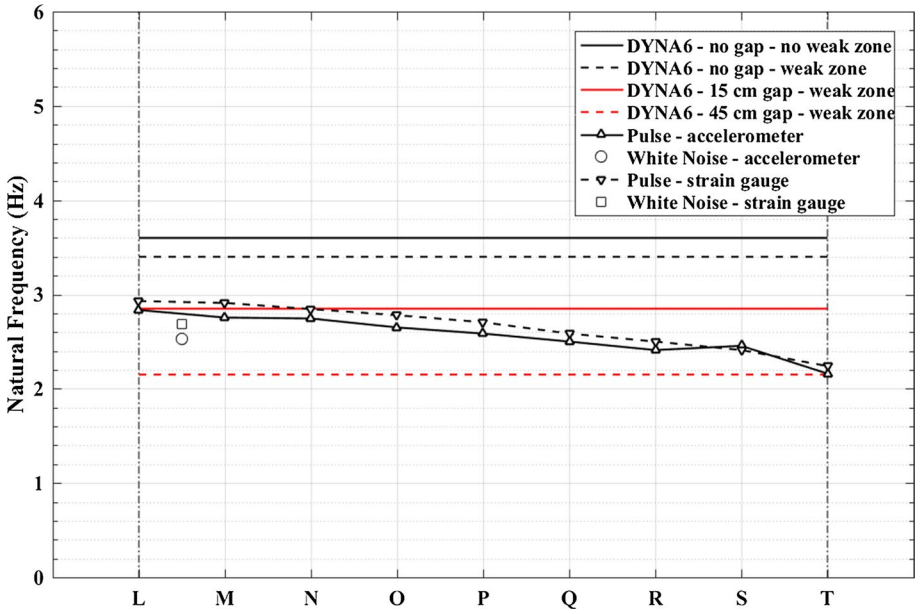

Fig. 23 Comparison of experimental natural frequency of P1 and DYNA6

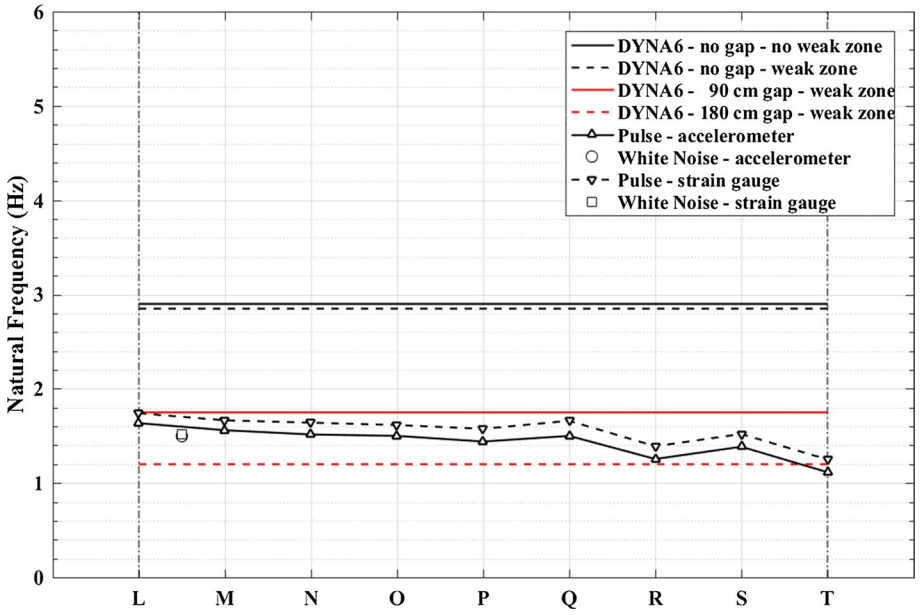

Fig. 24 Comparison of experimental natural frequency of P10 and DYNA6

can be noted from the figures, the calculated natural frequencies were far from the experimental values. This discrepancy could be attributed to weakening of the soil surrounding the pile and/or development of a gap along the upper part of the pile. Consequently, another

analysis was conducted considering a weak zone around the pile shaft (denoted DYNA6—no gap—weak zone) to account for the disturbance in the annular soil zone adjacent to the pile due to soil disturbance during pile installation and/or gap opening and closing at the pile-soil interface during shaking. This weak zone is characterized by its thickness as a ratio of pile's radius and reduced shear modulus as a ratio of the shear modulus of the undisturbed soil. The thickness ratio used corresponded to the soil column above the helix which was 1.88 and 0.82 for 88 mm piles and 140 mm piles respectively, and the shear modulus ratio was taken as 0.5. Even though the natural frequency decreased for the case of weak zone but was still much higher than the experimental results.

The observations made from monitoring the soil around the piles indicated the formation of a gap that varied between 15 and 50 cm, and in some cases, these gaps closed partially due to the soil caving in, resulting in loose soil zone around the piles (Allotey and El Naggar 2008). Therefore, further analyses were conducted considering gaps between the soil and the upper portion of the pile shaft. These gaps were modeled by increasing the free length of the pile. Due to successive shakings on TD2, although piles had no mass attached to their heads, soil around the pile experienced large deformations, and gaps opened around piles and the free length differed for each pile. DYNA6 models were established considering gaps of 15 cm and 45 cm for P1, and the results are presented in Fig. 23. The calculated natural frequencies from these cases are in good agreement with the recorded responses at the beginning and end of TD3, respectively. This demonstrates that successive shakings during TD3 have promoted the formation of deeper gap around the pile.

P10 experienced more deformations during TD2 and TD3 shakings (especially during TAK earthquake which caused resonance) and experienced larger deformations due to its larger cross-section, pile head mass and free length, hence deeper gaps formed. This led to significant nonlinear deformations in the soil and very large gaps were observed at the end of testing. The results from DYNA6 models of P10 considering a gap of 90 cm (at the beginning of TD3) and 180 cm (at the end of TD3) bounded the experimental results as shown in Fig. 24. It is also noted that the difference between the cases with and without a weak zone is negligible because the thickness of soil column above the helix was small compared to P1 as the same helix diameter was used for both.

For all 88 mm diameter piles, the gap depth ranged from (15 to 45 cm), while for 140 mm piles, the gap depth ranged from (60 to 180 cm) depending on the pile-head mass and free length.

4.4 Pile groups

Two pile groups were formed on TD4; the first pile group (PG1) comprised four piles of 88 mm diameter, and the second pile group (PG2) comprised four piles of 140 mm diameter. Each pile group supported a cubic steel skid (box) filled with sand (pile cap). Each skid was fitted with two accelerometers located at the level of its center of gravity. The natural frequencies of the pile groups were determined from the responses measured by the two accelerometers as well as the top strain gauge in each of the piles. Figure 25 displays the FRF for PG2 in TD4. Several observations can be made from Fig. 25. The responses from the accelerometers and top strain gauges were in excellent agreement. The average of the two measurements can be used to define the natural frequency. The FRF curve exhibits a large peak associated with the first natural frequency of PG2 and two smaller peaks corresponding to the natural frequencies of the sand bed, which manifest the effect of SSI.

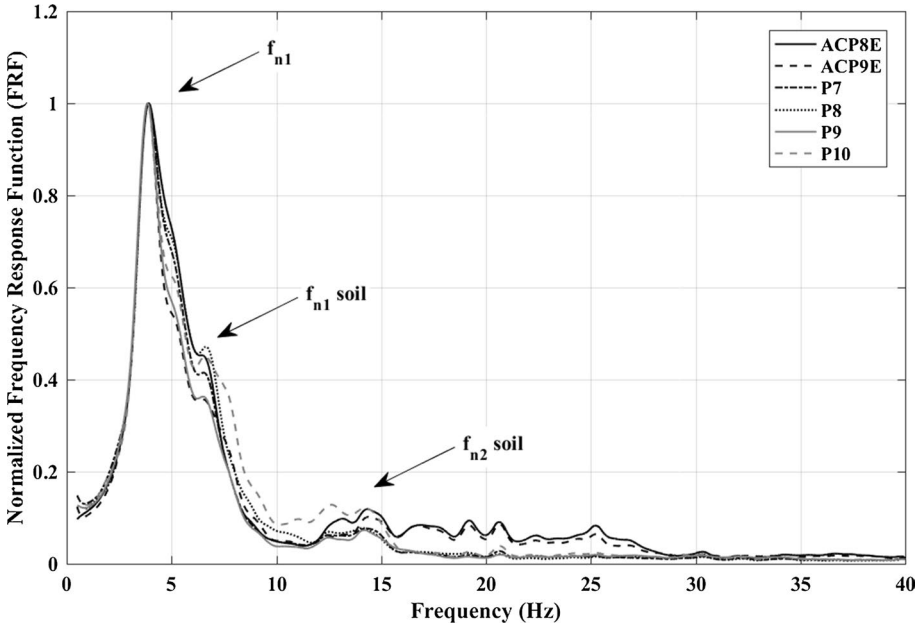

Fig. 25 Normalized FRF for PG2 due to white noise on TD4 (fixed connection)

However, this effect is smaller than what was observed for single piles. The pile group's behavior was dominated by the horizontal vibration mode because the rocking natural frequency was outside the frequency range of the white noise signal (0–40 Hz).

4.4.1 Effect of pile head's connection

Two pile-head conditions were simulated in the testing program. On TD4, each pile was connected to the steel kid using two bolts so as to simulate a fixed head. On TD5, one bolt was removed from each connection in order to simulate pinned connection. However, a true pin connection was not achieved and the one bolt connection still provided some restraint to pile heads.

The responses of PG2 with fixed head and pinned head connections are shown in Fig. 26. As noted from Fig. 26, the natural frequency of PG2 decreased as the pile head condition changed from fixed (two bolts) to pinned (one bolt). However, the difference is small between the two values because the one bolt still provided restraint to the pile head rotation. This would be further verified by comparing the natural frequency with the results from DYNA6.

4.4.2 Combined effect of stiffness, mass and free length

Since both pile groups had different pile cap masses (6350 kg for PG1 and 9979 kg for PG2), different pile diameters (i.e., different flexural stiffness) and different free lengths above the ground surface (1.17 m for PG1 and 1.73 m for PG2), the natural frequencies of the two groups cannot be compared directly. However, a combined effect of stiffness, pile

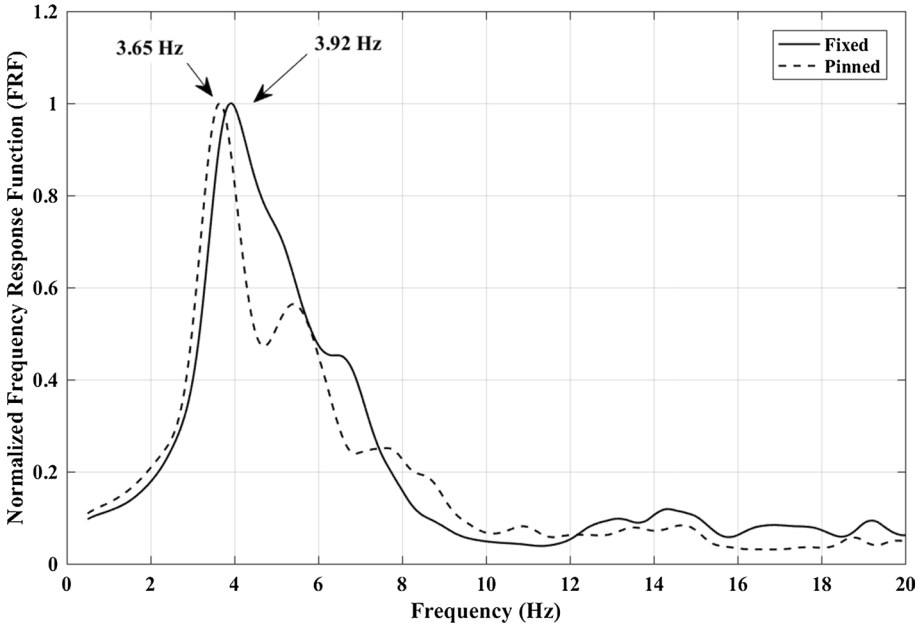

Fig. 26 Comparison between fixed and pinned head connection for PG2

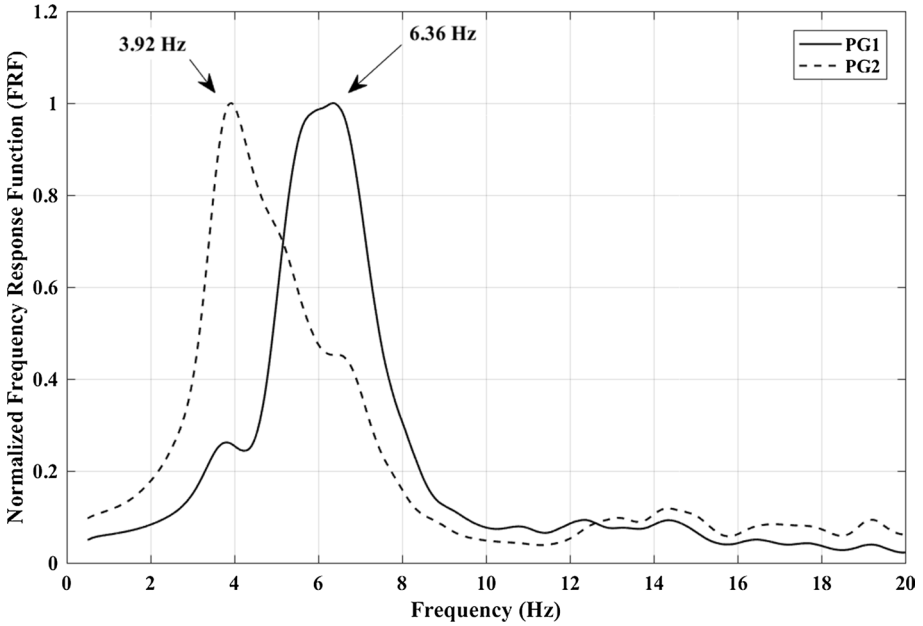

Fig. 27 Natural frequency of PG1 and PG2 on TD4 (fixed connection)

cap mass as well as free length can be compared. Figure 27 compares the FRF of PG1 and PG2 on TD4 (fixed pile head). Figure 27 shows that, although PG1 comprised small diameter piles, its natural frequency was nearly double that of PG2. The natural frequency of PG2 adjusted using Eq. 6 to account for the different mass effect would be 4.91 Hz, which is lower than that of PG1. Noting that the moment of inertia of PG2 piles was 7.5 times that of PG1 piles, but the free length of PG2 was larger than that of PG1, which resulted in a natural frequency lower than that of PG1. The same results were observed in single piles response, which illustrates the important effect of the free length (and the development of a gap) on natural frequency of pile-soil systems.

4.4.3 Summary of natural frequencies of pile groups

Table 7 presents the fundamental frequencies computed from accelerometers as well as strain gauges using both FFT and FRF for both pile head conditions. It is noted from Table 7 that the differences between the FFT and FRF results were generally less than 2%, except for PG1 in TD4 (fixed connection) were the difference was about 5%. Furthermore, the results obtained from the accelerometer and strain gauges responses were in good agreement. Table 7 also shows that the difference of fundamental frequency between fixed and pinned pile heads cases was about 5%, which clearly indicates that even one bolt provided sufficient restraint against rotation. This is an important observation as in many cases bolted connection of pile heads to steel skids supporting vibrating equipment is considered as pinned, which results in gross underestimation of the stiffness of the piled foundation and the natural frequency of the system. This can also have an important effect on the response of the system to seismic loading depending on the frequency content of the earthquake signal.

4.4.4 Effect of successive shakings

Responses of PG1 and PG2 to pulse waves were investigated to evaluate the effect of successive shaking on their natural frequencies. Figure 28 shows the variation of the fundamental frequency of PG1 and PG2 through TD4 (Pulse (U) to Pulse (CC)) and TD5 (Pulse (DD) to Pulse (MM)) calculated from measurements of the pile cap accelerometers as well

Table 7 Fundamental frequencies of fixed and pinned pile groups

Pile Group	f_{n1} (Hz)		Fixed		Pinned	
			FFT	FRF	FFT	FRF
PG1	Accelerometers	ACP3E	6.09	6.41	5.91	5.94
		ACP5E	6.09	6.36	5.75	5.86
	Strain Gauges	P1	6.09	6.38	5.78	5.87
		P2	6.07	6.34	5.61	5.84
		P3	6.05	6.44	5.89	5.93
		P4	6.11	6.34	5.09	5.96
PG2	Accelerometers	ACP8E	3.97	3.92	3.69	3.65
		ACP9E	3.88	3.86	3.37	3.53
	Strain Gauges	P7	3.94	3.89	3.68	3.63
		P8	3.95	3.9	3.69	3.64
		P9	3.89	3.86	3.37	3.53
		P10	3.90	3.87	3.36	3.56

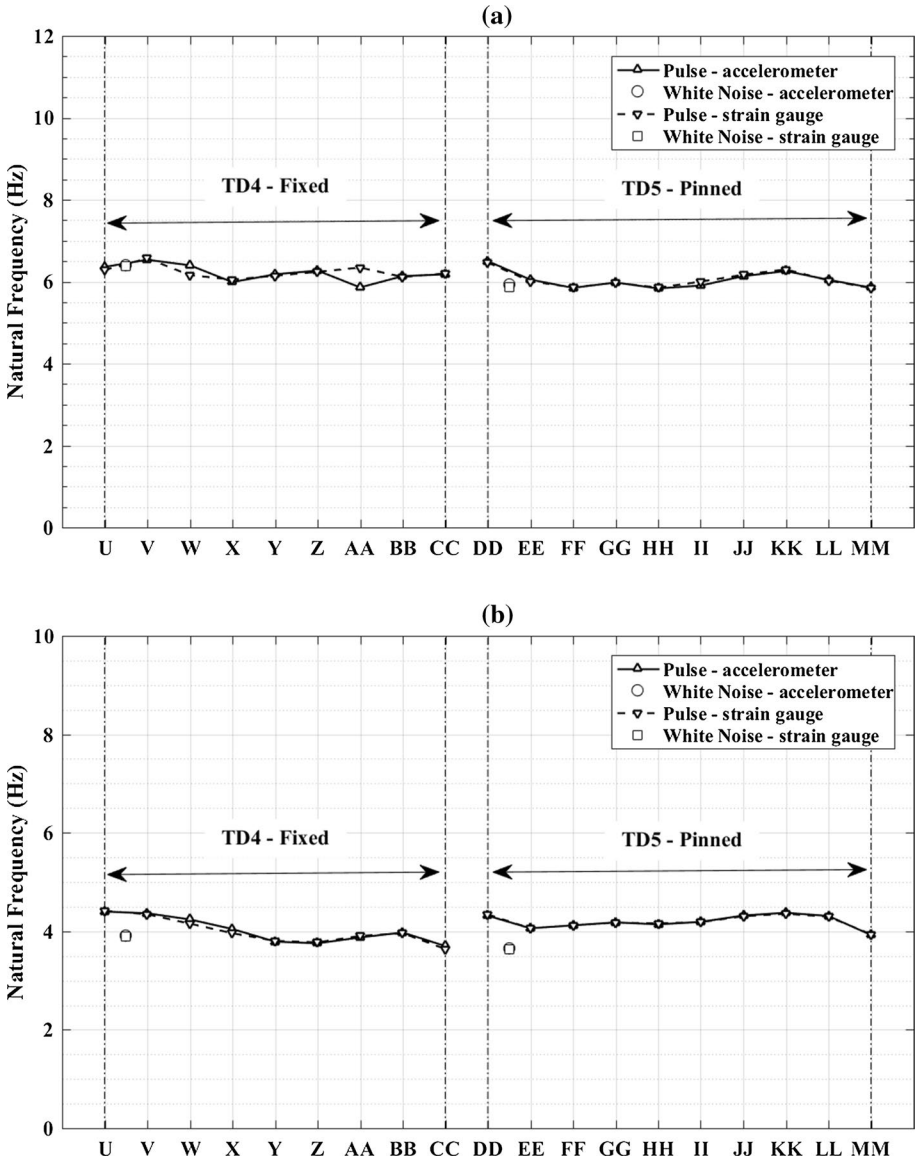

Fig. 28 Variation in natural frequencies of pile groups with successive shakings during TD4 and TD5: **a** PG1; **b** PG2

as the top strain gauge in one of the piles. Several observations can be made from these results. The value of natural frequency obtained from the response to pulse waves was generally higher than that computed from the response to white noise signals. It is also noted that the natural frequency decreased after each successive shaking, especially during TD4 because the fixed pile group experienced larger responses, which led to stronger soil nonlinearity and gapping. Hence, the stiffness and natural frequency of the system decreased. This reduction was even more pronounced for PG2 than for PG1 for the fixed pile groups.

This was because the closeness of the natural frequency of PG2 to the predominant frequency range of NOR earthquake signal, while the natural frequency of PG1 was outside that range. This means PG2 experienced significant resonance, which resulted in higher deflections. Figure 28 also shows that the natural frequency decreased the most in the first half of TD4 (NOR earthquake testing) then remained nearly constant afterwards. On the other hand, neither of the groups experienced resonance during TAK earthquake shakings because its predominant frequency range was lower than their natural frequencies. Thus, the natural frequency did not decrease during TAK shakings.

Table 8 provides a summary of the spectral accelerations for both pile groups. It is observed from Table 8 that the spectral acceleration for PG2 during NOR earthquake was very large (1.5–1.75 g) as its natural frequency was close to the predominant frequency range of NOR earthquake; however, the natural frequency of PG1 was outside that range and hence the spectral acceleration was lower. On the other hand, both pile groups had low spectral accelerations during TAK earthquake as their natural frequencies were far from the predominant frequency of TAK earthquake.

4.4.5 Comparison with DYNA6 program

The dynamic characteristics of pile groups PG1 and PG2 were evaluated employing DYNA6 software. DYNA6 accounts for pile-soil-pile interaction within a pile group using frequency dependent dynamic interaction factors employing the superposition approach (El Naggar and Novak 1995). In addition, it can account for the actual dimensions of the pile cap and free lengths of piles. Two models were established considering the geometrical properties of PG1 and PG2 and pile cap information. Pile caps were modeled as blocks with their actual dimensions of 2.13 m × 2.13 m × 1.73 m (L × W × H) and the applied masses of 6350 kg and 9979 kg for PG1 and PG2, respectively. The piles were arranged in square configuration with a center-to-center spacing of 1.07 m in both directions.

Different conditions were considered in the DYNA6 models to simulate the observed nonlinear response of the pile groups. This included considering a weak zone around the piles and/or gap opening along the top part of the piles. The calculated natural frequencies from DYNA6 models are compared with experimental values in Fig. 29.

The calculated natural frequency of the fixed pile groups obtained from DYNA6 models had the same trends as those observed from the analysis of single piles. The model considering linear behaviour (no weak zone or gap) resulted in high natural frequencies. The model that simulated nonlinearity by defining a weak zone around pile shafts resulted in slightly smaller natural frequency, especially for PG2. The model that simulated nonlinearity by introducing a gap of 15–30 cm provided natural frequency in good agreement with the experimental results for PG1. For PG2, the depth of the

Table 8 Spectral accelerations of PG1 and PG2

Pile group	Pile head condition	Fundamental frequency (Hz)	Fundamental period (s)	Spectral acceleration for NOR-100-T0 (g)	Spectral acceleration for TAK-100-T0 (g)
PG1	Fixed	6.38	0.157	0.89	0.85
	Pinned	5.90	0.169	1.00	1.05
PG2	Fixed	3.88	0.258	1.75	1.05
	Pinned	3.59	0.279	1.49	1.07

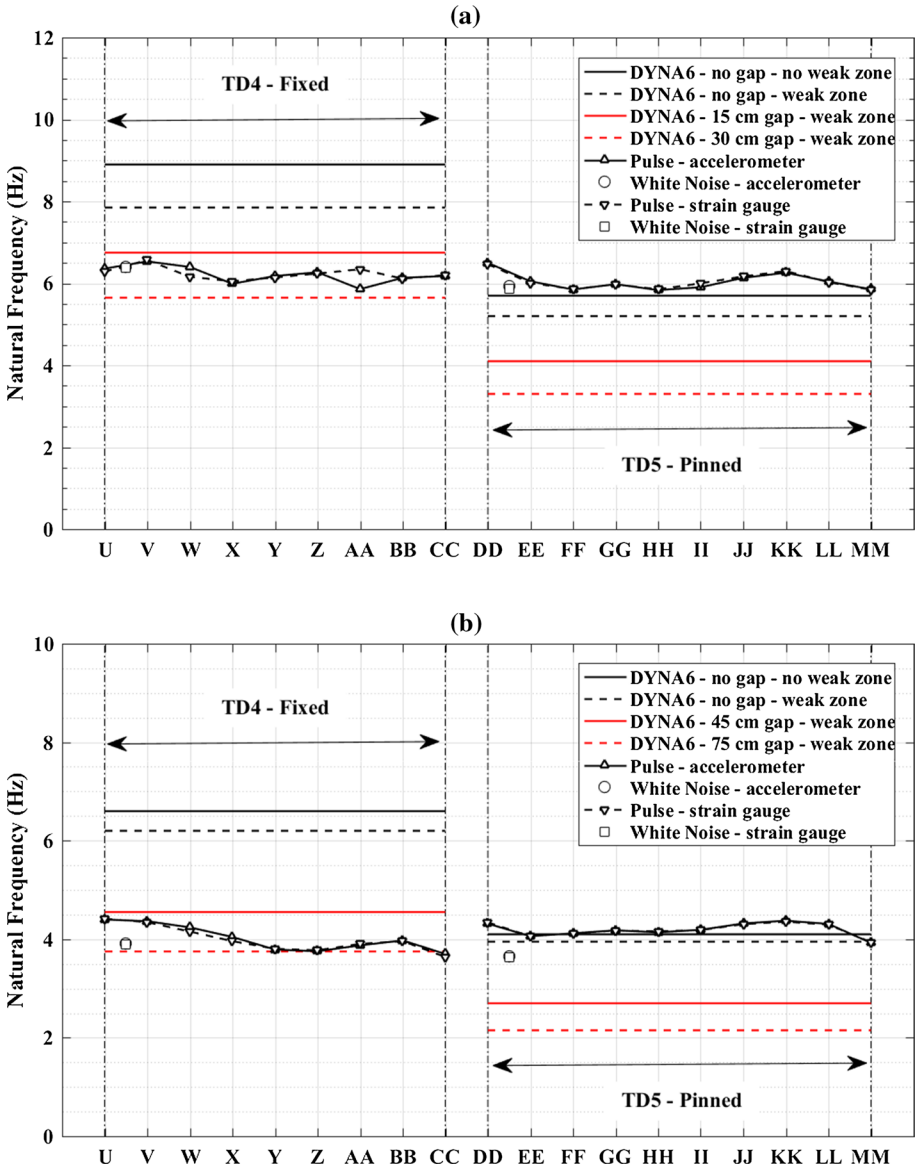

Fig. 29 Experimental and calculated natural frequencies for pile groups using DYNA6: **a** PG1; **b** PG2

gap was 45 cm at the beginning of TD4 and 75 cm at the end of the day to achieve a good match with the observed experimental results. The range of gap considered in the analysis was supported by test observations. The calculated natural frequency for pinned pile groups using DYNA6 models were lower than the experimental values even without considering a gap or weak zone around the pile shafts. Introducing a weak zone or a gap similar to the fixed head piles case, the natural frequency values were much smaller than the experimental results. This confirms that the one-bolt pile head connection cannot be considered as a pinned connection, and still provided some significant

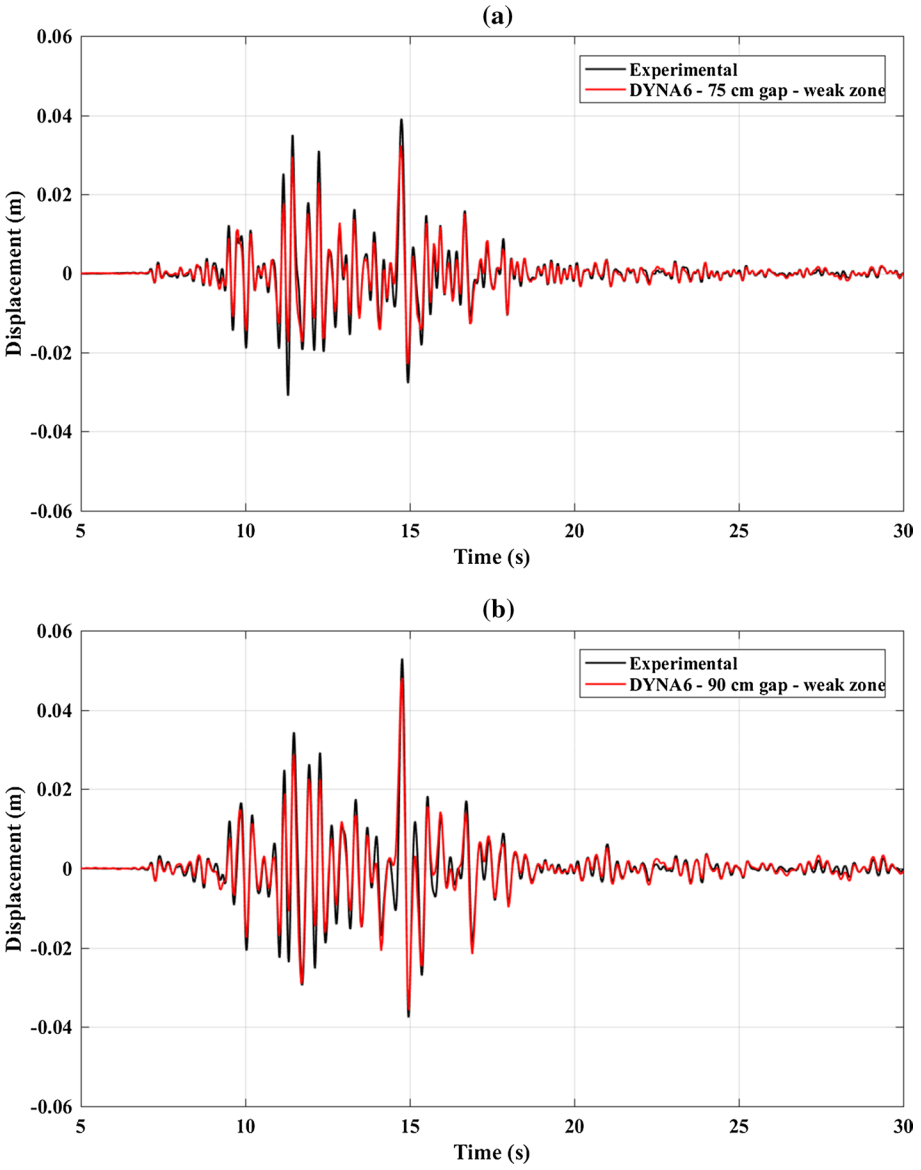

Fig. 30 Experimental and calculated response for pile groups due to NOR earthquake using DYNA6: **a** PG1; **b** PG2

rotational constraint, which resulted in higher lateral stiffness and correspondingly natural frequency.

In addition to capturing the correct dynamic properties of the pile groups, DYNA6 was employed to evaluate the responses of PG1 and PG2 due to NOR earthquake which are compared in Fig. 30 with the experimental results. The same considerations used in evaluating the natural frequency to simulate the nonlinearity in the soil were defined, i.e., a weak

zone and a gap. However, an excellent match between DYNA6 results and experimental results was achieved at a gap depth of 75 cm for PG1 and 90 cm for PG2, which were higher than those values introduced to capture the correct natural frequency. Since, natural frequencies obtained from the experimental results were due to pulse waves with low amplitude, higher shaking amplitudes during strong earthquakes would result in larger gap depths.

5 Conclusions

The following conclusions can be drawn from the shake table testing results as well as the analytical solutions for the single and grouped helical piles.

1. The stiffness and natural frequency of the sand bed increased due to pile installation and corresponding SSI. This was more pronounced in the case of pile groups. However, due to large responses during TD4 (pile groups testing), soil deformations increased causing degradation of soil's stiffness and gap forming along the upper portion of the piles, which reduced the natural frequency of the sand bed in the following day (TD5).
2. The number of helices increased the soil's disturbance during pile installation, which resulted in reduced pile's stiffness and natural frequency. On the other hand, as expected, increasing the pile's embedment depth and/or flexural stiffness increased its natural frequency.
3. Natural frequency of single piles and pile groups decreased due to successive shakings. This is attributed to the degradation in the pile-soil stiffness and opening of deeper gaps. However, in some cases the gap depth decreased due to sand caving-in after some additional shaking, which resulted in increases of stiffness and natural frequency.
4. The pile's free length significantly affects the stiffness of single and grouped helical piles. Gap opening further increases the free length and hence results in additional reduction in stiffness and natural frequencies. These effects must be considered in seismic design of helical pile foundations.
5. The DYNA6 software predicted the single and grouped piles behaviour by accounting for degradation of the soil's stiffness and gap opening. The gap depth ranged from (15 to 60 cm) for 88 mm single piles, (60–180 cm) for 140 mm single piles, (15–30 cm) for PG1 and (45 cm to 75 cm) for PG2. It is evident that the gap depth increased as the pile's diameter (and flexural stiffness) increased.
6. The seismic responses of single and grouped helical piles are greatly affected by the resonance condition (i.e., closeness of the natural frequency to the earthquake's predominant frequency). This leads to increased spectral accelerations causing larger deformations and decrease in the stiffness of the pile-soil system.
7. The observed behaviour of pile groups with a single-bolt connection indicated that the assumption of pin connection may not hold true in most cases, which can result in serious underestimation of the pile group's stiffness and hence can result in erroneous prediction of its response to seismic loading.

Acknowledgements The authors express their deep gratitude for the financial support received from Helical Pile and Tiebacks Committee (HPTC) members through the Deep Foundation Institute's (DFI) Special Projects Fund, as well as the National Science Foundation (NSF) (Grant No. 1624153). In addition, authors appreciate all the help donating, transporting and installing the piles, the concrete masses and the steel skids provided by Torcsill Foundations LLC, Ram Jack Foundation, Magnum Piering, Hubbell-Chance

and AMSquared Construction. The authors would also like to thank all the staff at the NEES/UCSD shaking table facility. Last but not least, the support provided by Almita Piling Inc. and MITACS is truly appreciated.

Funding Financial support for this research was provided by the Helical Pile and Tiebacks Committee (HPTC) members through the Deep Foundation Institute's (DFI) Special Projects Fund, as well as the National Science Foundation (NSF) (Grant No. 1624153).

Declarations

Conflict of interest The authors have no relevant financial or non-financial interests to disclose.

References

Albaghdadi TA, Brown MJ, Knappett JA, Ishikura R (2015) Modelling of laterally loaded screw piles with large helical plates in sand. In: Proceedings of the 3rd international symposium on frontiers in offshore geotechnics (Frontiers in Offshore Geotechnics III), Oslo, Norway, June 10–12, 2015, pp 503–508

Allotey N, El Naggar MH (2008) A numerical study into lateral cyclic nonlinear soil-pile response. Can Geotech J 45(9):1268–1281. https://doi.org/10.1139/T08-050

Alwalan MF, El Naggar MH (2020a) Finite element analysis of helical piles subjected to axial impact loading. Comput Geotech 123:103597. https://doi.org/10.1016/j.compgeo.2020.103597

Alwalan MF, El Naggar MH (2020b) Analytical models of impact force-time response generated from high strain dynamic load test on driven and helical piles. Comput Geotech 128:103834. https://doi.org/10.1016/j.compgeo.2020.103834

Badry P, Satyam N (2017) Seismic soil structure interaction analysis for asymmetrical buildings supported on piled raft for the 2015 Nepal earthquake. J Asian Earth Sci 133:102–113. https://doi.org/10.1016/j.jseaes.2016.03.014

Bagheri F, El Naggar MH (2013) Effects of installation disturbance on behaviour of multi-helix piles in sands. In: Proceedings of the 66th Canadian geotechnical conference (GeoMontreal 2013), Montreal, Canada, Sept. 30–Oct. 3, 2013, Paper No. 242

Bagheri F, El Naggar MH (2015) Effects of installation disturbance on behaviour of multi-helix piles in structured clays. DFI J J Deep Found Inst 9(2):80–91. https://doi.org/10.1179/1937525515Y.0000000008

Bhattacharya S, Lombardi D, Dihoru L, Dietz MS, Crewe AJ, Taylor CA (2011) Model container design for soil–structure interaction studies. In: Fardis M, Rakicevic Z (eds) Role of seismic testing facilities in performance-based earthquake engineering, vol 22. Geotechnical, Geological, and Earthquake Engineering. Springer, pp 135–158. https://doi.org/10.1007/978-94-007-1977-4_8

Boulanger RW, Curras CJ, Kutter BL, Wilson DW, Abghari A (1999) Seismic soil-pile-structure interaction experiments and analyses. J Geotech Geoenviron Eng 125(9):750–759. https://doi.org/10.1061/(ASCE)1090-0241(1999)125:9(750)

Carbonari S, Morici M, Dezi F, Gara F, Leoni G (2017) Soil-structure interaction effects in single bridge piers founded on inclined pile groups. Soil Dyn Earthq Eng 92:52–67. https://doi.org/10.1016/j.soildyn.2016.10.005

Cerato AB, Vargas TM, Allred SM (2017) A critical review: state of knowledge in seismic behaviour of helical piles. DFI J J Deep Found Inst 11(1):39–87. https://doi.org/10.1080/19375247.2017.1414108

Elkasabgy M, El Naggar MH (2013) Dynamic response of vertically loaded helical and driven steel piles. Can Geotech J 50(5):521–535. https://doi.org/10.1139/cgj-2011-0126

Elkasabgy M, El Naggar MH (2015) Axial compressive response of large-capacity helical and driven steel piles in cohesive soil. Can Geotech J 52(2):224–243. https://doi.org/10.1139/cgj-2012-0331

Elkasabgy M, El Naggar MH (2018) Lateral vibration of helical and driven steel piles installed in clayey soil. J Geotech Geoenviron Eng 144(9):06018009. https://doi.org/10.1061/(ASCE)GT.1943-5606.0001899

Elkasabgy M, El Naggar MH (2019) Lateral performance and p–y curves for large-capacity helical piles installed in clayey glacial deposit. J Geotech Geoenviron Eng 145(10):04019078. https://doi.org/10.1061/(ASCE)GT.1943-5606.0002063

El Naggar MH (2004) The 2002 colloquium address: the role of soil-structure interaction in foundation engineering. Can Geotech J 41(3):485–509. https://doi.org/10.1139/T04-014

El Naggar MH, Novak M (1994) Nonlinear lateral interaction in pile dynamics. Soil Dyn Earthq Eng 14(2):141–157. https://doi.org/10.1016/0267-7261(94)00028-F

El Naggar MH, Novak M (1995) Non-linear model for dynamic axial pile response. J Geotech Eng 120(2):308–329. https://doi.org/10.1061/(ASCE)0733-9410(1994)120:2(308)

El Naggar MH, Shayanfar MA, Kimiaei M, Aghakouchak AA (2005) Simplified BNWF model for non-linear seismic response analysis of offshore piles with nonlinear input ground motion analysis. Can Geotech J 42(2):365–380. https://doi.org/10.1139/T04-103

El Naggar MH, Novak M, Sheta M, El Hifnawi L, El Marsafawi H (2011) DYNA 6—a computer program for calculation of foundation response to dynamic loads. Western University, London, Ontario, Canada, Geotechnical Research Centre

Elsawy MK, El Naggar MH, Cerato A, Elgamal A (2019a) Seismic performance of helical piles in dry sand from large-scale shaking table tests. Géotechnique 69(12):1071–1085. https://doi.org/10.1680/jgeot.18.P.001

Elsawy MK, El Naggar MH, Cerato AB, Elgamal AW (2019b) Data reduction and dynamic p–y curves of helical piles from large-scale shake table tests. J Geotech Geoenviron Eng 145(10):04019075. https://doi.org/10.1061/(ASCE)GT.1943-5606.0002146

El Sharnouby MM, El Naggar MH (2018a) Field investigation of lateral monotonic and cyclic performance of reinforced helical pulldown micropiles. Int J Geomech 18(10):04018116. https://doi.org/10.1061/(ASCE)GM.1943-5622.0001161

El Sharnouby MM, El Naggar MH (2018b) Numerical investigation of axial monotonic performance of reinforced helical pulldown micropiles. Can Geotech J 55(10):1405–1420. https://doi.org/10.1139/cgj-2017-0330

Elsherbiny ZH, El Naggar MH (2013) Axial compressive capacity of helical piles from field tests and numerical study. Can Geotech J 50(12):1191–1203. https://doi.org/10.1139/cgj-2012-0487

Elsherbiny ZH, El Naggar MH, Elgamal AW (2017) Helical piles foundation for wind turbines: full-scale testing of a single helical pile in sand. In: Proceedings of the 3rd international conference on performance-based design in earthquake geotechnical engineering (PBD-III), Vancouver, Canada, July 16–19, 2017, Paper No. 488

Fahmy A, El Naggar MH (2016) Cyclic axial performance of helical-tapered piles in sand. DFI J J Deep Found Inst 10(3):98–110. https://doi.org/10.1080/19375247.2016.1211353

Fahmy A, El Naggar MH (2016) Cyclic lateral performance of helical tapered piles in silty sand. DFI J J Deep Found Inst 10(3):111–124. https://doi.org/10.1080/19375247.2017.1286428

Fahmy A, El Naggar MH (2017) Axial performance of helical tapered piles in sand. Geotech Geol Eng J 35(4):1549–1576. https://doi.org/10.1007/s10706-017-0192-1

Fleming BJ, Sritharan S, Miller GA, Muraleetharan KK (2015) Full-Scale seismic testing of piles in improved and unimproved soft clay. Earthq Spectra 32(1):239–265. https://doi.org/10.1193/012714EQS018M

Gavin K, Doherty P, Tolooiyan A (2014) Field investigation of the axial resistance of helical piles in dense sand. Can Geotech J 51(11):1343–1354. https://doi.org/10.1139/cgj-2012-0463

Givens MJ, Stewart JP, Haselton CB, Mazzoni S (2012) Assessment of soil-structure interaction modeling strategies for response history analysis of buildings. UCLA: Civil and Environmental Engineering. Accessed to https://escholarship.org/uc/item/019523j6

Guo Z, Deng L (2018) Field behaviour of screw micropiles subjected to axial loading in cohesive soils. Can Geotech J 55(8):34–44. https://doi.org/10.1139/cgj-2017-0109

Harnish J, El Naggar MH (2017) Large diameter helical pile capacity—torque correlations. Can Geotech J 54(7):968–986. https://doi.org/10.1139/cgj-2016-0156

Heidari M, El Naggar MH, Jahanandish M, Ghahramani A (2014) Generalized cyclic p–y curve modeling for analysis of laterally loaded piles. J Soil Dyn Earthq Eng 63(1):138–149. https://doi.org/10.1016/j.soildyn.2014.04.001

Jeremic B, Jie GZ, Preisig M, Tafazzoli N (2009) Time domain simulation of soil-foundation-structure interaction in non-uniform soils. J Earthq Eng Struct Dyn 38(5):699–718. https://doi.org/10.1002/eqe.896

Kagawa T, Sato M, Minowa C, Abe A, Tazoh T (2004) Centrifuge simulations of large-scale shaking table tests: case studies. J Geotech Geoenviron Eng 130(7):663–672. https://doi.org/10.1061/(ASCE)1090-0241(2004)130:7(663)

Kaynia AM (1982) Dynamic stiffness and seismic response of pile groups. Dissertation, Massachusetts Institute of technology

Kaynia AM, Kausel E (1982) Dynamic stiffness and seismic response of pile groups. MIT Report No. R82-03, Massechusetts Institute of Technology, Cambridge, Massachusetts

Lanyi-Bennett SA, Deng L (2019) Axial load testing of helical pile groups in galciolacustrine clay. Can Geotech J 56(2):187–197. https://doi.org/10.1139/cgj-2017-0425

Li W, Zhang DJY, Sego DC, Deng L (2018) Field testing of axial performance of large-diameter helical piles at two soil sites. J Geotech Geoenviron Eng 144(3):06017021. https://doi.org/10.1061/(ASCE)GT.1943-5606.0001840
Li W, Deng L (2019) Axial load tests and numerical modelling of single-helix piles in cohesive and cohesionless soils. Acta Geotech 14(2):461–475. https://doi.org/10.1007/S11440-018-0669-Y
Livneh B, El Naggar MH (2008) Axial testing and numerical modeling of square shaft helical piles under compressive and tensile loading. Can Geotech J 45(8):1142–1155. https://doi.org/10.1139/T08-044
Lou M, Wang H, Chen X, Zhai Y (2011) Structure–soil–structure interaction: Literature review. Soil Dyn Earthq Eng 31(12):1724–1731. https://doi.org/10.1016/j.soildyn.2011.07.008
Maheshwari BK, Truman KZ, El Naggar MH, Gould PL (2004) 3D FEM nonlinear dynamic analysis of pile groups for lateral transient and seismic excitations. Can Geotech J 41(1):118–133. https://doi.org/10.1139/T03-073
Maheshwari BK, Truman KZ, Gould PL, El Naggar MH (2005) Three-dimensional nonlinear seismic analysis of single piles using FEM: effects of plasticity of soil. Int J Geomech, ASCE 5(1):35–44. https://doi.org/10.1061/(ASCE)1532-3641(2005)5:1(35)
Michel P, Butenweg C, Klinkel S (2018) Pile-grid foundations of onshore wind turbines considering soil–structure-interaction under seismic loading. Soil Dyn Earthq Eng 109:299–311. https://doi.org/10.1016/j.soildyn.2018.03.009
Miura F (1997) Lessons from the damage caused by past earthquakes. International Workshop on Micropiles, Seattle, WA
Mostafa YE, El Naggar MH (2002) Dynamic analysis of laterally loaded pile groups in sand and clay. Can Geotech J 39(6):1358–1383. https://doi.org/10.1139/t02-102
Moss RES, Caliendo JA, Anderson LR (1998) Investigation of a cyclic laterally loaded model pile group. Soil Dyn Earthq Eng 17(7–8):519–523. https://doi.org/10.1016/S0267-7261(98)00003-7
Motamed R, Towhata I, Honda T, Tabata K, Abe A (2013) Pile group response to liquefaction-induced lateral spreading: E-Defense large shake table test. Soil Dyn Earthq Eng 51:35–46. https://doi.org/10.1016/j.soildyn.2013.04.007
Mylonakis G, Gazetas G (2000) Seismic soil-structure interaction: beneficial or detrimental? J Earthq Eng 4(3):277–301. https://doi.org/10.1080/13632460009350372
Nabizadeh F, Choobbasti AJ (2019) Field study of capacity helical piles in sand and silty clay. Transp Infrastruct Geotechnol 4:3–17. https://doi.org/10.1007/s40515-016-0036-06
Newgard JT, McCartney JS, Schneider JA, Thompson DJ (2019) Static and cyclic axial loading of single and multiplate helical anchors in sand. In: Proceedings of the 1st international symposium on screw piles for energy applications, Dundee, UK, May 27–28, pp 81–86
Novak M (1974) Dynamic stiffness and damping of piles. Can Geotech J 11(4):574–598. https://doi.org/10.1139/t74-059
Novak M, Aboul-Ella F (1978) Impedance functions of piles in layered media. J Eng Mech, ASCE 104(EM3):643–661
Perez ZA, Schiavon JA, Tsuha CHC, Dias D, Thorel L (2018) Numerical and experimental study on influence of installation effects on behaviour of helical anchors in very dense sand. Can Geotech J 55(8):1067–1080. https://doi.org/10.1139/cgj-2017-0137
Perko HA (2009) Helical piles: a practical guide to design and installation, 1st edition
Ridgley N (2015) Practice note 28: Screw piles: Guidelines for design, construction & installation. The Institution of Professional Engineers New Zealand (IPENZ)
Sakr M (2009) Performance of helical piles in oil sand. Can Geotech J 46(9):1046–1061. https://doi.org/10.1139/T09-044
Sakr M (2011) Installation and performance characteristics of high capacity helical piles in cohesionless soils. DFI J J Deep Found Inst 5(1):39–57. https://doi.org/10.1179/dfi.2011.004
Schiavon JA, Tsuha CHC, Thorel L (2017) Cyclic and post-cyclic monotonic response of a single-helix anchor in sand. Géotech Lett 7(1):11–17. https://doi.org/10.1680/jgele.16.00100
Schiavon JA, Tsuha CHC, Neel A, Thorel L (2019) Centrifuge modelling of a helical anchor under different cyclic loading conditions in sand. Int J Phys Modell Geotech 19(2):72–88. https://doi.org/10.1680/jphmg.17.00054
Seed HB, Idriss IM (1970) Soil moduli and damping factors for dynamic response. Report No. EERC 70–10, Earthquake Engineering Research Center, University of California, Berkeley, California, p 40
Seed HB, Lysmer J (1978) Soil-structure interaction analyses by finite elements—State of the art. Nucl Eng Des 46(2):349–365. https://doi.org/10.1016/0029-5493(78)90020-1
Shahbazi M, Cerato AB, Allred S, El Naggar MH, Elgamal A (2019) Damping characteristics of full-scale grouped helical piles in dense sands subjected to small and large shaking events. Can Geotech J 57(6):801–814. https://doi.org/10.1139/cgj-2018-0769

Shahbazi M, Cerato AB, El Naggar MH, Elgamal A (2020) Evaluation of seismic soil-structure interaction of full-scale grouped helical piles in dense sand. Int J Geomech 20(12):04020228. https://doi.org/10.1061/(ASCE)GM.1943-5622.0001876

Shirato M, Nonomura Y, Fukui J, Nakatani S (2008) Large-scale shake table experiment and numerical simulation on the nonlinear behavior of pile-groups subjected to large-scale earthquakes. Soils Found 48(3):375–396. https://doi.org/10.3208/sandf.48.375

Stewart JP, Crouse CB, Hutchinson T, Lizundia B, Naeim F, Ostadan F (2012) Soil–Structure interaction for building structures. National Institute of Standards and Technology (NIST GCR 12-917-21)

Techno Metal Post (n.d.) Structures on helical piles withstand Alaska earthquakes. Accessed to https://www.technometalpost.com/en-CA/structures-supported-by-techno-metal-post-helical-piles-withstand-2016-and-2018-alaska-earthquakes

Tsuha CHC, Aoki N, Rault G, Thorel L, Garnier J (2012) Evaluation of the efficiencies of helical anchor plates in sand by centrifuge model tests. Can Geotech J 49(9):1102–1114. https://doi.org/10.1139/T2012-064

Tweten DJ, Ballard Z, Mann BP (2014) Minimizing error in logarithmic decrement method through uncertainty propagation. J Sound Vib 333(13):2804–2811. https://doi.org/10.1016/j.jsv.2014.02.024

Xu C, Dou P, Du X, El Naggar MH, Miyajuma M, Chen S (2020a) Seismic performance of pile group-structure system in liquefiable and non-liquefiable soil from large-scale shake table tests. Soil Dyn Earthq Eng 138:106299. https://doi.org/10.1016/j.soildyn.2020.106299

Xu C, Dou P, Du X, El Naggar MH, Miyajuma M, Chen S (2020b) Large shaking table tests of pile-supported structures in different ground conditions. Soil Dyn Earthq Eng 139:106307. https://doi.org/10.1016/j.soildyn.2020.106307

Authors and Affiliations

A. F. Fayez[1] · M. H. El Naggar[1] · A. B. Cerato[2] · A. Elgamal[3]

A. F. Fayez
afayez@uwo.ca

A. B. Cerato
acerato@ou.edu

A. Elgamal
aelgamal@ucsd.edu

[1] Department of Civil and Environmental Engineering, Western University, London, ON N6A 3K7, Canada

[2] School of Civil and Environmental Science, University of Oklahoma, Norman, OK 73019, USA

[3] Department of Structural Engineering, University of California – San Diego, La Jolla, CA 92093, USA